Doctoral Dissertation

Photodynamic Therapy for Cancer using Mitochondrial Drug Delivery System

(ミトコンドリア薬物送達システムを用いた癌光線力学療法の検証)

Satrialdi

Graduate School of Life Science, Hokkaido University

2020, March

PHOTODYNAMIC THERAPY FOR CANCER USING MITOCHONDRIAL DRUG DELIVERY SYSTEM

ミトコンドリア薬物送達システムを用いた癌光線力学療法の検証

By

SATRIALDI

A dissertation submitted to Hokkaido University in partial fulfilment of the requirements for the degree of
Doctor of Philosophy

2020

HOKKAIDO
UNIVERSITY

Laboratory for Molecular Design of Pharmaceutics
Faculty of Pharmaceutical Sciences
Graduate School of Life Science
Hokkaido University
Japan

PHOTODYNAMIC THERAPY FOR CANCER USING MITOCHONDRIAL DRUG DELIVERY SYSTEM

ミトコンドリア薬物送達システムを用いた癌光線力学療法の検証

SATRIALDI

Supervisor

Prof. Hideyoshi Harashima

Yuma Yamada, Ph.D.

[ABSTRACT]

A non-invasive and specific targeting for cancer therapy is a necessity to manifest in order to minimize the harmful effect on the non-malignant cells. During the past century, photodynamic therapy (PDT) has been actively developed as a non-invasive approach to effectively eradicate the cancer cells with minimal effect on healthy cells. The PDT effect is derived from an energy transfer reaction between light as a source of energy to molecular oxygen, mediated by a light-activated molecule, known as the photosensitizer. The dynamic interaction among these three major components in PDT produces a lethal level of reactive oxygen species (ROS), mainly singlet oxygen. The selectivity of this therapy could be achieved by the specific accumulation of the non-toxic photosensitizer in the tumor region, accompanied by the precise delivery of light in the corresponding area. The singlet oxygen has a highly reactive characteristic that can readily react with several vital molecules in the biological system, resulting in the molecule dysfunction. This interaction may also lead to irreversible oxidative damage and further provoke a lethal effect for the cells. However, the harmful effects of singlet oxygen are restricted by their short lifetime and inadequate diffusion capacity. Therefore, the specific delivery of photosensitizer, mainly in organelle-level, could be a promising strategy to obtain the maximum benefits of this therapy. Moreover, as the important organelle that holds both the vital and lethal functions, mitochondria are identified to be an attractive target for optimizing the PDT outcomes.

In the current condition, the existing photosensitizers often manifest disadvantageous features for a practical PDT application. One of them is a non-specific accumulation either in the cellular or at the subcellular level. The other drawback is the inadequate ability of most photosensitizers in absorbing near-infrared (NIR) light. The application of NIR light in PDT, especially in the optical window of biological tissues, is profoundly beneficial because NIR light has an excellent penetration ability toward tissue consisting of water and biomolecules. These problems restrict the use of such compounds in clinical applications. Therefore, the development of a novel PDT system that can fulfill the requirements of the selective organelle accumulation in combination with the long-wavelength light activation is inevitable.

The main objective of this research was to construct a novel mitochondrial targeting PDT system with the long-wavelength light activation process. To realize that goal, a synergistic combination between a π-extended porphyrin-type photosensitizer, namely rTPA, and a MITO-

Porter system, a versatile mitochondrial targeting liposomal-based nanodevice, was introduced. The incorporation of the rTPA compound into the MITO-Porter system was accomplished using the hydration method with the resulting particle showed a homogenous distribution with a diameter of 157 ± 7 nm and highly positive zeta potentials of 32 ± 3 mV. This novel mitochondrial targeting PDT system, namely the rTPA-MITO-Porter, manifested a robust capacity in producing a high level of singlet oxygen, specifically in the mitochondrial compartment of tumors, during a 700-nm light irradiation process. Based on the cellular uptake and intracellular observation results, most of the rTPA-MITO-Porter particles were efficiently internalized into the cells and concentrated in the mitochondrial compartment of tumors. Furthermore, this system displayed an efficient cytotoxicity profile against two types of human tumor cell lines, namely HeLa cells (human cervical cancer cells) and SAS cells (human squamous cells carcinoma of the tongue), as indicated by the low EC_{50} value of 0.16 ± 0.02 μM and 0.41 ± 0.18 μM, respectively. Additionally, the apoptosis pathway was actively induced during the PDT process of the rTPA-MITO-Porter, as shown by the formation of apoptotic bodies and fragmentation of mitochondrial structure.

Inspired by the excellent cell killing ability during the *in vitro* experiments, the translation process into the *in vivo* applications has further proceeded. A slight modification on the rTPA-MITO-Porter formulation, particularly on the helper lipid composition and the total lipids' concentration, was made without altering the mitochondrial targeting ability and the photo-induced cytotoxic capacity. The remarkable inhibition of the tumor growth was obtained in the SAS cells-bearing mouse model after a single PDT treatment of the rTPA-MITO-Porter with the rTPA dose of 8.2 μg/mouse *via* intratumoral administration. There was also no significant alteration on the bodyweight of the mice during the treatment, implying the promising *in vivo* cell-killing ability of this system with a high safety profile. Furthermore, the depolarization on the mitochondrial membrane was observed after the PDT process of the rTPA-MITO-Porter, indicating the damage of mitochondrial membrane due to the specific localization of the photochemical reaction on the mitochondrial compartment of tumors. Finally, the findings presented in this research serve to verify the considerable functions of the MITO-Porter system as the mitochondrial selective drug delivery technology in potentiating the PDT outcomes as well as the importance of mitochondria as the predominant subcellular target for PDT. Moreover, this novel biologically-active nanomaterial manifests an encouraging feature for PDT applications, particularly for the superficial-type cancer cells.

[DECLARATION]

I declare that the work presented in this dissertation was carried out by myself except for the collaborative contributions that have been indicated explicitly and acknowledged. The research was conducted under the supervision of Prof. Hideyoshi Harashima and Yuma Yamada, Ph.D., in the Laboratory for Molecular Design of Pharmaceutics, Faculty of Pharmaceutical Sciences, Hokkaido University, Japan. I also confirm that this work has not been submitted for any other degree or professional qualification at this or any other university.

Satrialdi

March, 2020

[ABBREVIATION]

5-ALA	5-aminolevulinic acid
ATP	Adenosine triphosphate
CHEMS	Cholesteryl hemi succinate
Chol	Cholesterol
CLSM	Confocal laser scanning microscopy
CPP	Cell penetrating peptide
DLI	Drug-light interval
DLS	Dynamic light scattering
DMEM	Dulbecco's modified eagle medium
DMSO	Dimethylsulfoxide
DOPE	1,2-dioleoyl-*sn*-glycero-3-phosphatidylethanolamine
EC_{50}	The minimum concentration required to eliminate half of the cell population
EPC	Non-hydrogenated egg phosphatidyl choline
ERK	Extracellular signal-regulated kinase
ETC	Electron transport chain
FACS	Fluorescence-activated cell sorting
FBS	Fetal bovine serum
FDA	U.S. Food and Drug Administration
GSH	Glutathione
HBG	HEPES buffer containing glucose
IMM	Inner mitochondria membrane
IMS	Intermembrane space
MAPK	Mitogen-activated protein kinase
MFI	Mean fluorescence intensity
NBD	N-(7-nitro-2-1,3-benzoxadiazol-4-yl)
NBD-DOPE	N-(7-nitro-2-1,3-benzoxadiazol-4-yl) labeled DOPE
NIR	Near-infrared
PALS	Phase analysis light scattering
PBS	Phosphate-buffer saline
PCC	Pearson's correlation coefficient

PDT	Photodynamic therapy
PET	Photoinduced electron transfer
PS	Photosensitizer
R8	Octaarginine peptide, a cell-penetrating peptide
rTPA-LPs	rTPA in unmodified liposomes (DOPE:SM)
ROS	Reactive oxygen species
SM	Sphingomyelin
SOSG	Singlet oxygen sensor green
STR-R8	Stearylated octaarginine
TMRM	Tetramethylrhodamine methyl esther

[ACKNOWLEDGEMENT]

I would like to express my sincere gratitude to my supervisors, Prof. Hideyoshi Harashima and Yuma Yamada, Ph.D., for their continued support, guidance, motivation, and inspiration throughout this doctoral research project. I am especially indebted to Yuta Takano, Ph.D. (associate professor at Research Institute for Electronic Science, Hokkaido University), who has been actively encouraged me to pursue the goals of this research. I wish to extend my special thanks to Prof. Mikako Ogawa, the chairman of my dissertation committee, for her great support and invaluable advice.

I wish to show my appreciation to all teachers in the Laboratory for Molecular Design of Pharmaceutics, Takashi Nakamura Ph.D., Yusuke Sato, Ph.D., and Ikramy A. Khalil, Ph.D., for their scientific advice and many insightful discussions. My thanks go out to all members of the Laboratory for Molecular Design of Pharmaceutics, for helping and encouraging me to finalize this project. More specifically, I would like to acknowledge Shinnosuke Daikuhara and Reina Munechika, who have been supported me in commencing this research.

Most importantly, I wish to express my very profound appreciation to my parents, Akmal and Rifliwita, my lovely wife, Narissa Anugrawati, and my adorable daughter, Sheza Azzahra Keinarra, who always provide unfailing support and energy for me in conducting and writing this dissertation.

Exceptional gratitude belongs to Indonesia Endowment Fund for Education (LPDP), Ministry of Finance of the Republic of Indonesia, and Ministry of Research, Technology, and Higher Education of the Republic of Indonesia for the scholarship support, which made it possible for me to complete this doctoral research project.

[TABLE OF CONTENTS]

CHAPTER 1

General Introduction

CHAPTER 1
GENERAL INTRODUCTION

1.1 General Introduction

As the primary energy factories for the cells, mitochondria play an indispensable role in the synthesis process of the energy-rich molecule adenosine triphosphate (ATP). The synthesis process of ATP is mainly located in the cristae of the inner mitochondria membrane (IMM), acknowledged as oxidative phosphorylation. This process comprises the movement of the electrons through several protein complexes subsequently with the proton motive across the IMM to the intermembrane space (IMS). During this electron transport process, a small number of electrons could escape and react immaturely with the oxygen molecules to form the reactive oxygen species (ROS), specifically superoxide ($O2^{\bullet-}$), which rapidly transformed into hydrogen peroxide (H_2O_2) by superoxide dismutase. Basically, cells are equipped by a defense mechanism system to control the amount of ROS below the concentration that could harm the cells. At a certain level, ROS play an important role in the intracellular signaling pathways to regulate several biological and physiological processes (1). However, moderately increment of ROS level causes genetic instability, which may promote the transformation and progression of cancers (2). Furthermore, due to the highly reactive characteristic of ROS, the uncontrolled production of ROS may induce an irreversible oxidative damage and further produce lethal effects for the cells (3).

The current report suggested that the mitochondrial ROS play a significant role in the cell signaling process that controls cell proliferation *via* the regulation of mitogen-activated protein kinase/extracellular signal-regulated kinase (MAPK/ERK) pathway (4). Interestingly, the increment of the ROS level in malignant cells is accompanied by the expansion of the scavenging activity of the endogenous antioxidant systems. Glutathione (GSH), an endogenous tripeptide (glutamate, cysteine, and glycine) antioxidant, was discovered in the higher level in some cancer cells as opposed to the non-malignant tissues, as well as another antioxidant system, specifically thioredoxin (5,6). The increase in antioxidant activity is associated with cancer initiation and progression. Therefore, the inhibition of this antioxidant activity was observed to be beneficial to overcome tumor progression and metastasis (7–9). Furthermore, the antioxidant supplementation could further accelerate the progression and metastasis of several cancer cells (10–12).

ROS possess a highly reactive characteristic, particularly with numerous major biologically active molecules such as proteins, lipids, and nucleic acids, following in the dysfunction of the molecules. This intrinsic and harmful nature of ROS could be exploited as a powerful weapon for cancer therapy by promoting the massive production of ROS selectively in tumor cells. Several methods have been developed to elevate the production of ROS in cancers, such as depleting the antioxidant activity (13,14), inhibiting the mitochondrial respiratory system (15), and generating an excessive amount of ROS *via* photochemical reaction, specifically photodynamic therapy (PDT). The latter effort exhibits a highly spatiotemporal selectivity towards tumor cells, making it more encouraging contrasted to the other efforts.

By definition, PDT is an innovative approach for treating solid tumors using a combination of a non-toxic light-activated molecule (photosensitizer) and a harmless visible light in the presence of oxygen molecules to produce a lethal level of ROS (16,17). PDT was first introduced by Oscar Raab in the early of the 1900s. He accidentally recognized the notable toxic effect of the combination of acridine and light toward paramecium. Furthermore, the first endeavor regarding the application of PDT for cancer therapy was initiated by Herman von Tappeiner, who took over Raab's work to treat skin tumors using the white light irradiation of topically-administered eosin (17,18). Since the approval of the first photosensitizer for cancer PDT at the end of the 20th century under the brand name of Photofrin®, the PDT grows as an active research field due to the encouraging features of PDT, particularly the highly selective effect on the tumors through the dual selectivity concept (19). Several photosensitizers have been approved for clinical application (**Table 1.1**), while others are currently in the clinical trial.

Table 1.1 Clinically approved photosensitizer

Photosensitizer	Trade name	Excitation wavelength (nm)	Manufacture	Application
Porfimer sodium	Photofrin®	630	Axcan Pharma, Canada	Oesophageal, endobronchial, brain, cervical, bladder, gastric, lung tumors
5-aminolevulinic acid (5-ALA)	Levulan®, Ameluz®	635	DUSA, USA	Actinic keratosis, basal-cell carcinoma, head and neck, bladder tumors
5-ALA-methylester	Metvix®	570-670	Galderma, UK	Non-hyperkeratotic actinic keratosis, basal cell carcinoma
Temoporfin	Foscan®	652	Biolitec, Germany	Advanced head and neck cancer
Verteporfin	Visudyne®	690	Novartis, Switzerland	Basal-cell carcinoma, age-related macular degeneration
Talaporfin	Laserphyrin®	664	Meiji Seika, Japan	Glioma, lung, oesophageal cancer
Padeliporfin	Tookad®	753	Steba Biotech, Luxembourg	Prostate cancer

*References: (20,21)

The PDT effect is resulted from the dynamic interaction between photosensitizer, light, and oxygen molecule, leading to the production of the harmful level of ROS (**Figure 1-1**). In brief, the photosensitizer harvests the photon energy from the specific wavelength of light and utilize the energy to excite one electron into the higher energy level of the excited singlet state (S_1). Naturally, the molecule tends to go back into the most stable state of ground singlet state (S_0) and emit some energy in the form of light (fluorescence) or thermal (internal conversion). Alternatively, the exciting photosensitizer may undergo the intersystem crossing to the more stable triplet state (T_1). In this state, the photosensitizer could interact with the surrounding substrates and transfer the electron to produce superoxide followed by the generation of peroxide and hydroxyl radicals. This reaction is known as a Type 1 or electron transfer reaction.

Another possibility, which is the most common mechanism in cancer PDT, is the Type 2 or energy transfer reaction, where the photosensitizer immediately transfers the energy into the molecular oxygen ($^3O_2$) to form the highly reactive singlet oxygen (19,22,23). The specific location of the photochemical reaction may significantly affect the therapeutic outcomes of PDT. It is due to the nature of singlet oxygen that has a very short lifetime (~48 ns) and limited diffusion capacity (~20 nm) (24).

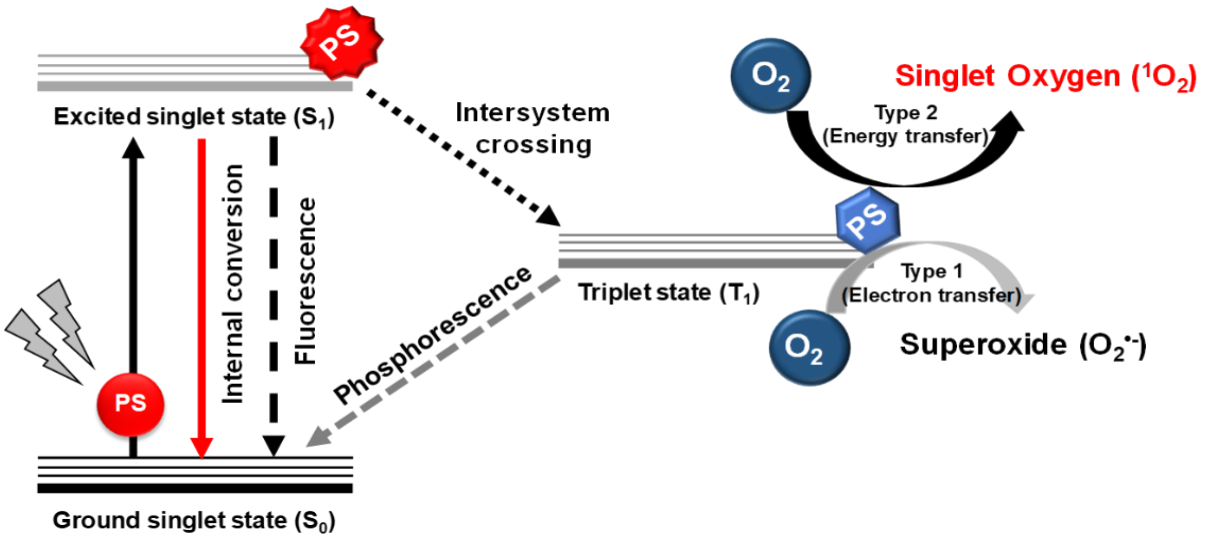

Figure 1-1 Conceptual illustration of mechanism during the photodynamic process. *Photosensitizer plays an essential role as an energy mediator to carry the photon energy from light to the molecular oxygen through the intersystem crossing process. The excessive energy is utilized by the oxygen to produce a reactive species that could readily react with several important biological molecules.*

Photosensitizer plays an essential function during the PDT process as an energy mediator between the light source and oxygen molecule. The ideal photosensitizer should meet some criteria as follows: (1) a pure and stable substance which only has the cytotoxic characteristic in the presence of suitable wavelength of light; (2) accumulate dominantly in the target tissue either in cellular or subcellular level and have low systemic toxicity; (3) have a high quantum yield for photochemical event, usually for the production of singlet oxygen; and (4) have a high extinction coefficient at the absorption wavelength around 600-850 nm to obtain the maximum tissue penetration capacity with minimum light scattering effect (25,26). However, in the current state, it is challenging to find single photosensitizer that meets the requirements mentioned above. Therefore, the development of a novel PDT system is needed to potentiate the therapeutic benefits and to minimize the adverse effects.

Over the last several decades, mitochondria have drawn much attention in cancer therapy due to their fundamental role as the key player on the programmed cell death (apoptosis) and as the bioenergetic engine to support the cell activities, especially on the high energy-demanded malignant cells. Mitochondria are also known to be the primary source of ROS (27), particularly during the oxidative phosphorylation process. Moreover, mitochondria are the most active oxygen consumer among the other organelles (28), as the primary fuel for the aerobic respiration to support their fundamental role as the primary energy factory for the cells. All the facts mentioned above concerning the importance role of mitochondria suggest that these rod-shaped organelles can be acknowledged as the potential target for PDT.

To date, several investigations have been reported regarding the significance of mitochondria targeting in the PDT field. For instance, the mitochondria delivery of chlorin e6, a widely used photosensitizer, resulted in higher effectivity for cancer therapy as opposed to the non-mitochondrial targeting system (29). It was also reported that the specific delivery of verteporfin, an FDA-approved photosensitizer, into the mitochondria of human KB cells led to the activation of the apoptotic pathway (30), a more desirable for the cancer therapy due to the negligible inflammation effects, which would lessen the side effects for healthy cells. Moreover, the mitochondrial accumulation of iridium (III) advanced the PDT outcome in the hypoxic condition (31). However, most of the recent reports on the mitochondrial targeting PDT are based on the chemical conjugation of the existing photosensitizers with the mitochondria-specific ligand, which may diminish the light-harvesting ability of the parent compound. Moreover, some of the reported mitochondrial targeting PDT systems required a short wavelength of light in combination with high light dose to activate the photosensitizer, which is not favored for the clinical application.

It is well known that mitochondria possess the highest membrane potential among the other organelles in a cell and that it readily interacts with the cations. According to the Nernst equation, the mitochondrial membrane potential of living cells could promote the uptake of the cations, resulting in a 100-1000 fold higher concentration compared to the cytoplasm (32). This characteristic has been exploited to deliver various compounds into mitochondria through electrostatic interactions with the positive charge carrier or molecule. Nevertheless, an electrostatic interaction is not adequate to realize an efficient delivery into mitochondria. The lipid composition or lipophilicity of the molecule should also be considered as an indispensable factor in intensifying mitochondrial accumulation to promote infiltration into the mitochondrial membrane.

Our group previously reported on the development of a unique mitochondrial targeting liposomal-based nanodevice called a MITO-Porter system (33,34). The nanocarrier was composed of mitochondrial fusogenic lipid of dioleoyl-sn-glycero-3-phosphatidylethanolamine (DOPE) and sphingomyelin (SM) with the cell-penetrating peptide of octaarginine (R8) on the exterior of the liposomes. The R8 surface modification has two specific functions, to stimulate the cellular uptake process *via* macropinocytosis (35) and to force the interaction with the mitochondria membrane through electrostatic interactions (33,34,36). The MITO-Porter system has been employed to deliver a wide range of molecules, ranging from hydrophilic to hydrophobic compounds, selectively into the mitochondrial compartment of living cells for several targeting purposes. It has also been used to deliver an electron donor-acceptor linked molecule consisting of a porphyrin core into mitochondria of HeLa cells to control the intracellular redox reaction with the photoactivation process at 430-440 nm (37). These findings indicate the promising capacity of the MITO-Porter system as the most potential mitochondria selective drug delivery system to be employed in the PDT applications.

Porphyrin is the most popular class of photosensitizers that have been extensively used in the clinical application due to their excellent ability to induce the formation of singlet oxygen through the photoirradiation process. However, the porphyrin compounds exhibit poor ability in harvesting long-wavelength light, resulting in the limitation on the application of this compound (38). In this research, I introduced a new generation of porphyrin-type photosensitizers, namely rTPA, as a potential candidate to be incorporated into the MITO-Porter system. The rTPA is an original compound, synthesized by Yuta Takano, Ph.D., an associate professor at Research Institute for Electronic Science, Hokkaido University. This compound was developed through the π-electron conjugation of the porphyrin structure using two triarylamine moieties to reconstruct the photophysical properties of the porphyrin structure (**Figure 1-2**).

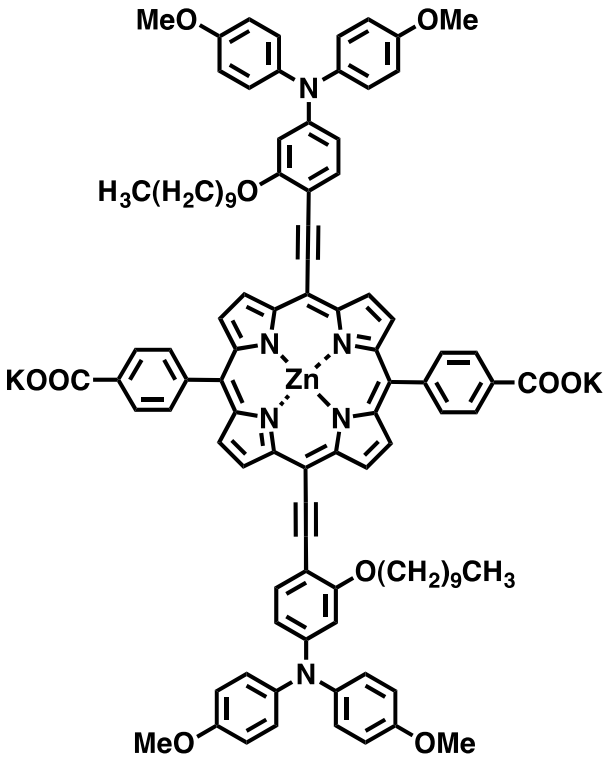

Figure 1-2 Chemical structure of rTPA compound*. This compound consists of metallated-porphyrin core with the π-electron conjugation using two triarylamine moieties.*

The effectivity of this π-elongation can be observed through the presence of the sharp absorption peak at near-infrared (NIR) region (absorptivity molar (ε) = 6.2 x 10^4 M^{-1} cm^{-1} at 704 nm in DMSO), while no absorption band was recognized in the case of basic porphyrin compound (**Figure 1-3**). The ability of rTPA in harvesting long-wavelength light is an advantage in the PDT application to have a better penetration ability toward tissues containing water and biomolecules. The specific delivery of this new generation of porphyrin compound into the mitochondrial compartment of tumors could be a promising approach to have the full potential of this compound. Therefore, the MITO-Porter system was employed in carrying and directing this compound selective into the mitochondrial compartment of tumors. Moreover, by encapsulating the rTPA into the MITO-Porter system, this compound could be dispersed in the monomeric phase on the aqueous solution, which is essential for the effective photochemical reaction.

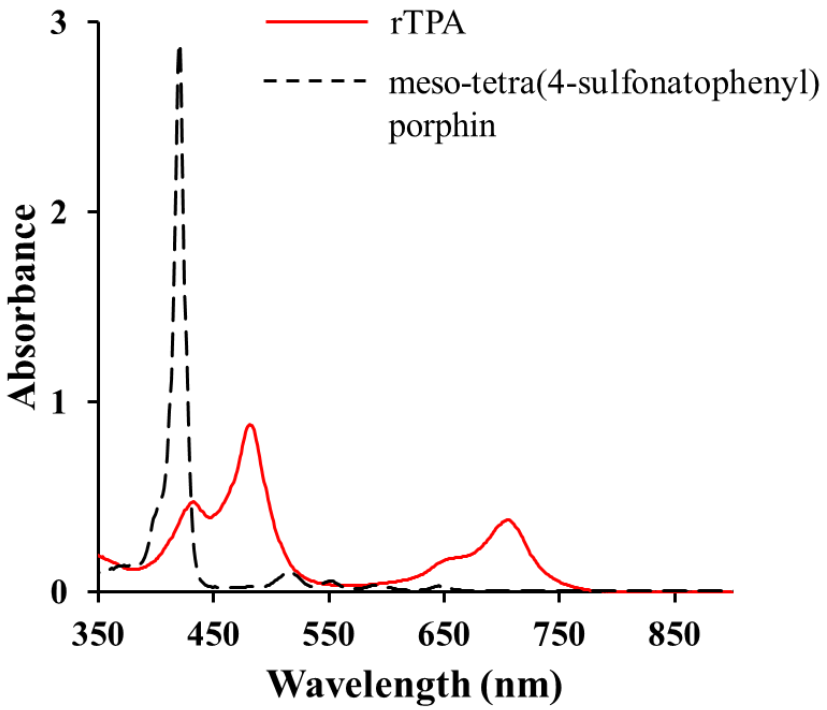

Figure 1-3 Absorption spectra of rTPA and basic porphyrin compound*. The rTPA compound shows a significant red-shift compared to the basic porphyrin compound, as a result of the π-electron conjugation on the porphyrin structure.*

1.2 Research Objectives

The main objective of this research was to construct a novel mitochondrial targeting PDT system with the long-wavelength light activation process. A synergistic combination strategy between a newly synthesized photosensitizer and a liposomal-based nanocarrier was introduced to achieve this objective, as shown in **Figure 1-4**. This system was composed of a π-extended porphyrin-type photosensitizer, rTPA, which has an excellent ability to induce the production of a high-level of singlet oxygen during 700-nm light irradiation process in combination with a versatile mitochondrial targeting nanodevice, namely MITO-Porter system. A series of *in vitro* experiments were conducted to validate the PDT concept and effectivity of this system. Furthermore, the potential application of this system was verified in the human cancer-bearing mouse model.

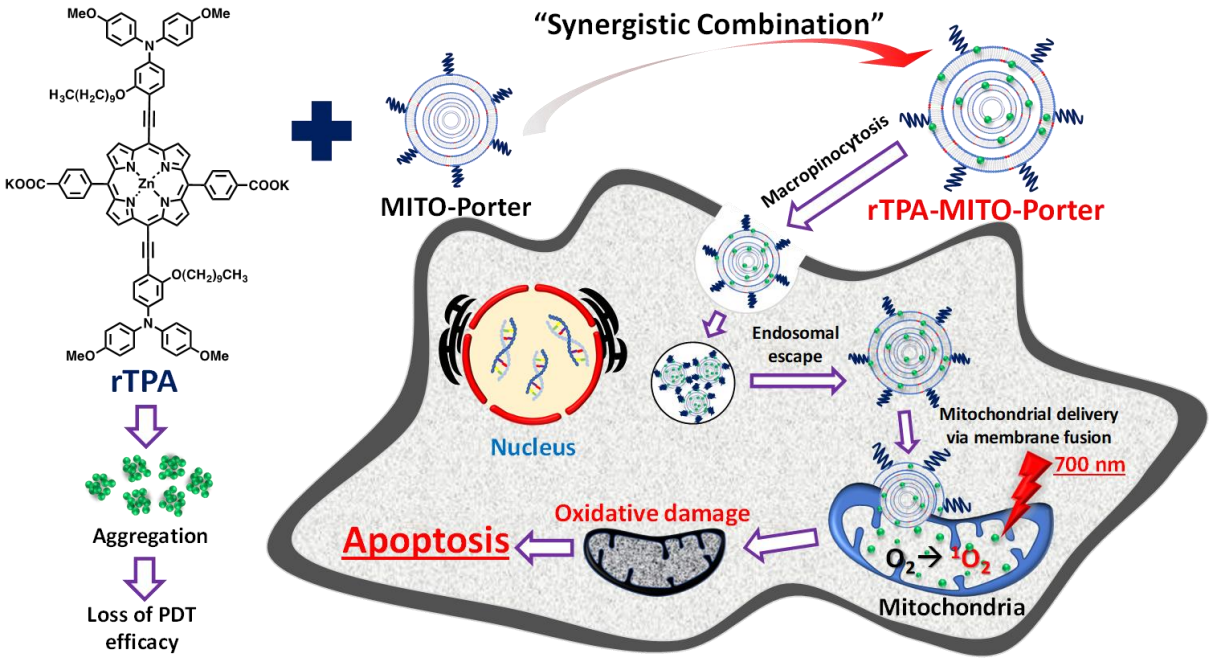

Figure 1-4 Schematic illustration of the research strategy. *The mitochondrial delivery of rTPA compound could be achieved by the incorporation into the MITO-Porter system (rTPA-MITO-Porter). The rTPA-MITO-Porter could be taken up by the cells via macropinocytosis followed by electrostatic interaction and membrane fusion process with negatively charged mitochondria membrane. The 700-nm light activates the rTPA; then the activated rTPA interacts with the molecular oxygen to generate a toxic level of singlet oxygen, leading to the irreversible oxidative damage which may induce the apoptosis cell death. In the free form, the rTPA tends to form aggregate, particularly in the aqueous solution, due to the highly hydrophobic characteristics of this compound, resulting in the loss of PDT effectivity.*

1.3 Outline of Dissertation Book

This dissertation book is divided into four chapters. Chapter 1 provides a comprehensive introduction as the background of this research. The classical problems of conventional PDT system are discussed in this chapter, particularly regarding the non-specific accumulation profile of the existing PDT systems followed by inadequate capacity of the majority of photosensitizers in absorbing long-wavelength photon energy. A synergistic combination approach is proposed as a promising strategy to improve the PDT therapeutic outcomes, by employing a new generation of the porphyrin-type photosensitizer with the versatile mitochondria targeting drug delivery system.

The construction process of the novel mitochondrial targeting PDT system and the characterization of the particles are reported in Chapter 2. This characterization consists of the physical characteristics and biological behavior, including the photophysical properties of the particles. At the end of this chapter, the PDT effectivity is reported by evaluating the cell-killing ability during the PDT process and validating the cell death mechanism.

In Chapter 3, the translation process from the *in vitro* settings to the *in vivo* application is reported. Slightly modification on the rTPA-MITO-Porter formulation was made by changing the helper lipid composition and increasing the total lipids' concentration. The purpose of this formulation design is to obtain adequate particle integrity with a suitable amount of encapsulated rTPA that meets the requirement for *in vivo* application. The mitochondrial delivery and its PDT activity were validated against SAS cells as the target cancer cells. The *in vivo* antitumor activity was then evaluated in the SAS cells-bearing mouse model. Finally, in the last chapter of this book, the general conclusion is presented with several potential directions for the further development of this novel-biologically active nanomaterial.

CHAPTER 2

Construction of Novel Mitochondria Targeted PDT System

CHAPTER 2
CONSTRUCTION OF NOVEL MITOCHONDRIA TARGETED PDT SYSTEM[1]

The novel mitochondria targeting PDT system was constructed by incorporating a π-extended porphyrin-type photosensitizer (rTPA) into the MITO-Porter system, a versatile mitochondrial targeting nanodevice. The rTPA compound was designed to possess sufficient solubility in solvents and dispersibility in the lipid bilayers of the nanocarrier and mitochondrial membrane (39). The π-electron conjugation using two triarylamine moieties was introduced into the porphyrin ring to synthesize the rTPA molecules, resulting in a significant alteration on the photophysical properties of the porphyrin compound. One of the significant improvements of this newly-synthesized photosensitizer is its capacity in harvesting photons from long-wavelength light, specifically at around 700 nm. However, this compound has a highly hydrophobic characteristic that tends to form aggregates, particularly in the aqueous solution. The aggregation of the porphyrin structure leads to the decrease of the singlet oxygen quantum yield, consequently loss of PDT efficacy (40–42).

Since the discovery of the first liposomal system by Alec D. Bangham and co-workers in the 1960s (43), this technology has been extensively developed as the most valuable drug-carrier system for several biomedical applications. A liposome is constructed from biocompatible and biodegradable materials such as natural lipids and non-toxic phospholipids. A liposomal system consists of one or more hydrophobic phospholipid bilayer membrane that encloses the hydrophilic aqueous core. This amphiphilic characteristic offers the appropriateness of liposomal nanocarrier for carrying both hydrophilic and hydrophobic compounds. Moreover, the incorporation of drugs into the liposomal system could improve the stability of the drug (44–46). Therefore, the incorporation of the rTPA compound into lipid bilayers of the liposomal system could minimize the possibility to form aggregate and further improve the stability of this compound. Furthermore, by employing the MITO-Porter system, the selective tumor mitochondrial delivery of the rTPA compound could be realized to attain the maximum PDT efficacy.

[1] Parts of this chapter have been published on:
Satrialdi, Munechika R., Biju V., Takano Y., Harashima H., & Yamada Y., The optimization of cancer photodynamic therapy by utilization of a pi-extended porphyrin-type photosensitizer in combination with MITO-Porter, *Chem. Commun.*, 2020, **56**, 1145-1148, DOI: 10.1039/C9CC08563G

This chapter covers the formulation development of the novel mitochondrial targeting PDT system, namely the rTPA-MITO-Porter, including the characterization and *in vitro* PDT evaluation in order to validate the therapeutic concept and its effectivity. The characterization process consists of the evaluation of the physical characteristics, photophysical properties, and biological performance of the particles. The physical characteristics consist of the evaluation of the particle size and its distribution, zeta potential, and encapsulation efficiency. The ability to provoke the production of singlet oxygen and other types of ROS during the photoactivation process was evaluated in order to understand the photophysical properties of this system. Moreover, the cellular uptake efficiency and intracellular trafficking manner of the particles on the living cells were evaluated as a part of the particle interaction behavior with the biological system. Finally, the effectivity of this system was assessed in the *in vitro* settings by evaluating the PDT cytotoxicity against two different types of human cancer cells, followed by the validation of the cell death mechanism.

2.1 Experimental Procedures

2.1.1 Materials

The 1,2-dioleoyl-*sn*-glycero-3-phosphatidylethanolamine (DOPE), and sphingomyelin (SM) were obtained from Avanti Polar Lipids, Inc. (Alabaster, AL, USA). Non-hydrogenated egg phosphatidyl choline (EPC) was purchased from NOF Corporation (Tokyo, Japan). Stearylated-R8 (STR-R8) was obtained from Toray Research Center, Inc. (Tokyo, Japan). The rTPA compound was synthesized by Yuta Takano, Ph.D. Dulbecco's Modified Eagle Medium (DMEM) and fetal bovine serum (FBS) were obtained from Wako (Osaka, Japan) and Sigma Aldrich Corp. (St. Louis, MO, USA), respectively. SAS cells, human oral squamous carcinoma cells, were received from National Institutes of Biomedical Innovation, Health, and Nutrition JCRB Cell Bank (Osaka, Japan). HeLa cells, human cervical cancer cells, were collected from Riken BRC (Tsukuba, Japan). The premix WST-1 Cell Proliferation Assay System kit was obtained from Takara Bio Inc. (Shiga, Japan). All additional chemicals and solvents used were purchased as commercially available reagent-grade products.

2.1.2 Construction of the PDT System

The rTPA in chloroform solution was sonicated for one minute to break the aggregate. The solution was transferred into a 1.5 mL tube; then, the solvent was removed and replaced with the DMSO followed by sonication for 15 s. The rTPA concentration was measured using a spectrophotometer with the maximum absorption wavelength at 704 nm. This concentration was used to calculate the initial amount of rTPA for the preparation of nanoparticles.

The incorporation of the rTPA compound into the MITO-Porter system was carried out using the hydration method. Briefly, the lipid films were prepared by mixing 0.55 mM lipids in ethanol with a molar ratio of 9:2 of DOPE:SM and 5 mol% of rTPA in chloroform followed by solvent evaporation. The resulting lipid films were hydrated using 500 μL of 10 mM HEPES buffer supplemented with 290 mM glucose (pH 7.4) followed by 15 minutes incubation at room temperature. The hydrated lipid film was sonicated for 45 seconds using a bath-type sonicator. To remove the non-encapsulated drug, the suspension was centrifuged at 20,600 x g for 5 minutes; then, the supernatant was collected. The STR-R8 solution (10 mol% of the total lipids) was added to the suspension to produce the rTPA-MITO-Porter. The rTPA compound was also incorporated into EPC-SM-R8 nanocarrier using a similar method as described above.

The particle size and its distribution were analyzed using dynamic light scattering (DLS) method, while zeta potential was measured using the patented technique of phase analysis light scattering (PALS) called M3-PALS technology (Zetasizer Nano ZS, Malvern Instruments, Worcestershire, UK). To calculate the encapsulation efficiency, the rTPA encapsulated in the liposomes containing N-(7-nitro-2-1,3-benzoxadiazol-4-yl) labeled DOPE (NBD-DOPE) was freeze-dried for one night. The obtained powder was dissolved in DMSO, followed by the measurement of the absorbance of rTPA using a spectrophotometer at the wavelength of 704 nm. The concentration of lipids was determined by measuring the fluorescence intensity of NBD (ex/em: 550/590 nm). The encapsulation efficiency was calculated using the following equation:

$$encapsulation\ efficiency\ (\%) = \frac{recovered\ rTPA / recovered\ lipid}{initial\ amount\ of\ rTPA / initial\ amount\ of\ lipid} \times 100$$

2.1.3 Photoinduced Singlet Oxygen Generation Ability

The detection of singlet oxygen production using Singlet Oxygen Sensor Green (SOSG) reagent (Thermo Fischer Scientific Inc.; Waltham, MA, USA) was carried out following the manufacture's protocol. In brief, a mixture of 2 μM rTPA in nanocarrier and 5 μM of SOSG solution were irradiated using a Xenon lamp (MAX-303, Asahi Spectra; Tokyo, Japan) at the wavelength of 700 ± 6 nm (20 mW/cm^2). The change in fluorescence intensity of the solutions at 530 nm was measured using a spectrofluorometer with an excitation wavelength of 490 nm. The meso-tetra(4-sulfonatophenyl) porphin was used as a positive control with 430-nm light irradiation to activate the molecule.

2.1.4 Cell Culture

HeLa cells and SAS cells were cultured in low glucose of DMEM supplemented with 10% FBS and penicillin-streptomycin under an atmosphere condition of 5% CO_2/air at 37 °C. The cell passage was performed at 90% confluency. The cell stocks were preserved in a cell banker solution with a concentration of 1 x 10^6 cells/tube and stored at -80 °C.

2.1.5 Detection of ROS Generation in Mitochondria

The *in vitro* singlet oxygen and superoxide levels were determined using Si-DMA (Dojindo Molecular Technologies Inc.; Kumamoto, Japan) and MitoSOX™ Red Mitochondrial Superoxide Indicator (Thermo Fischer Scientific Inc.), respectively. HeLa cells were seeded on a 35-mm glass base dish (Iwaki; Osaka, Japan) 24 h prior to the experiment. The rTPA-nanocarriers with 0.1 μM rTPA were transfected for 1 h in a serum-free medium, followed by 2 h in medium containing 10% FBS. The probe solution was added, followed by a 45 minutes and 10 minutes of incubation for Si-DMA and MitoSOX™ Red, respectively. The fluorescence signal of the probe was detected using confocal laser scanning microscopy (CLSM, Olympus FV10i-LIV, Olympus Corporation; Tokyo, Japan) equipped with a water-immersion objective lens (UPlanSApo 60x/NA. 1.2) and a dichroic mirror (DM405/473/559/635). The cells were excited with a 559 nm light from an LD laser with the fluorescence detection channel at 570-620 to detect the MitoSOX™ Red signal, while, for Si-DMA, the excitation wavelength was set at 635 nm with the fluorescence detector at 660-710 nm. The CLSM observation was conducted before and after light irradiation (Xenon lamp, λ =

700 ± 6 nm, 68.5 mW/cm^2). The mean fluorescence intensity of Si-DMA was calculated using ImageJ software.

2.1.6 Cellular Uptake Analysis

The cells were implanted on 6-well plates (Corning Inc.; Corning, NY, USA) and maintained under an atmosphere of 5% CO_2/air at 37°C for 24 h. The NBD-labeled rTPA-nanocarrier was used as the sample and was transfected into the cells for 1 h in serum-free DMEM. The transfected cells were washed twice with phosphate buffer saline (PBS (-)) containing 20 units/mL of heparin followed by trypsinization. The detached cells were centrifuged at 700 x g at 4°C for 3 minutes, and the supernatant was removed. The cell pellet was washed with PBS (-) containing 0.5% (w/v) bovine serum albumin and 0.1% (w/v) sodium azide (FACS buffer) followed by centrifugation with the same conditions. The supernatant was discharged, and the cell pellet was resuspended in the FACS buffer. Cellular uptake was determined using a flow cytometer (Gallious, Beckman Coulter; Brea, CA, USA). The NBD fluorescent probe was excited by a 488 nm laser and detected with a fluorescent light sensor at 525 nm (FL1). The measurement results were expressed as the mean fluorescence intensity (MFI). At least three independent analyses were conducted.

2.1.7 Intracellular Trafficking Analysis

The cells were seeded on a 35-mm glass base dish 24 h before transfection. Cells were transfected with the sample (NBD-labeled rTPA-nanocarrier) in phenol red-free DMEM without serum for 1 h, followed by an additional 2 h incubation in phenol red-free DMEM supplemented with 10% serum. The cells were washed, and the medium was replaced with fresh phenol red-free DMEM containing serum and fluorescent reagents (MitoTracker^{TM} Deep Red FM) followed by 20 minutes of incubation. The observation was performed using Olympus FV10i-LIV equipped with a water-immersion objective lens (UPlanSApo 60x/NA. 1.2) and a dichroic mirror (DM405/473/559/635). The cells were illuminated with 473 nm light and 635 nm light to excite the NBD-labelled nanocarrier and the MitoTracker Deep Red FM, respectively. The two fluorescence detection channels were set using a filter at a bandpass 490-540 nm to detect NBD-labelled nanocarrier and bandpass 660-710 nm to detect MitoTracker^{TM} Deep Red FM. The quantification of the mitochondrial colocalization level was performed

from randomly-selected CLSM images using ImageJ software by calculating Pearson's correlation coefficient (PCC).

2.1.8 *In Vitro* PDT Evaluation

Cell viability was measured using the WST-1 assay. In brief, the cells were cultured on a 48-well plate (Corning Inc.) for 24 h. The sample was transfected into the cells in serum-free DMEM for 1 h, followed by the next 2 h in DMEM containing serum. The cells were washed using DMEM containing serum followed by the photoirradiation process using a Xenon lamp at the wavelength of 700 ± 6 nm. The WST-1 reagent was added to the cells immediately after irradiation, then incubated for 2 h. The change of the reagent absorbance was measured at 450 nm with the reference at 630 nm using a microplate photometer (EnSpire® Multimode Plate Reader, Perkin Elmer; Waltham, MA, USA). At least three independent evaluations were conducted.

2.1.9 Validation of Cell Death Mechanism

The cell death mechanism during the PDT process was determined by direct CLSM observation. The evaluation was carried out by staining the mitochondrial compartment using MitoTracker™ Deep Red FM. The NBD-labeled rTPA-nanocarrier was used and transfected for 1 h in phenol red-free DMEM without serum, followed by 2 h in phenol red-free DMEM containing serum. Changes in cell morphology were observed using a live imaging system during irradiation at a suitable excitation wavelength of rTPA sourced from a High-Speed Laser Confocal Microscopy Nikon-A1Rsi (Nikon Corporation; Tokyo, Japan) instrument. The microscope equipped with an oil-immersion objective lens (Plan Apo VC, 60x, NA 1.4) and the dichroic mirror (DM405/488/561/640). The cells were irradiated using the diode lasers with 487 nm light to excite the NBD-labeled rTPA-nanocarrier and 636 nm light to excite the MitoTracker™ Deep Red FM. The two fluorescence detection channels were set at 525/50 nm and 700/75 nm to detect the NBD-labeled rTPA-nanocarrier and MitoTracker™ Deep Red FM, respectively.

2.2 Results

2.2.1 Construction and Physical Characterization of the PDT System

The rTPA-MITO-Porter system was constructed using a lipid mixture of DOPE and SM with a molar ratio of 9:2 through the hydration method, followed by surface modification with the cell-penetrating peptide of STR-R8 (**Figure 2-1**). The resulting nanoparticles exhibited a homogenous particle size with a highly positively-charged characteristic indicated by the positive zeta potential value of 32 ± 3 mV. This characteristic is derived from the occupation of the highly positively-charged octaarginine (R8) fractions on the exterior of the particles. The attachment of R8 moieties on the surface of MITO-Porter was achieved through hydrophobic interactions between the stearyl chain of STR-R8 and lipid bilayer of liposomes. Before the addition of STR-R8, negatively-charged nanoparticles (rTPA-LPs) were obtained. Furthermore, the rTPA compound was also incorporated into the non-mitochondrial targeting nanoparticles comprising of EPC and SM with R8 surface modification (33,34). All the liposomal preparation of rTPA manifested comparable particle properties, as displayed in **Table 2.1**.

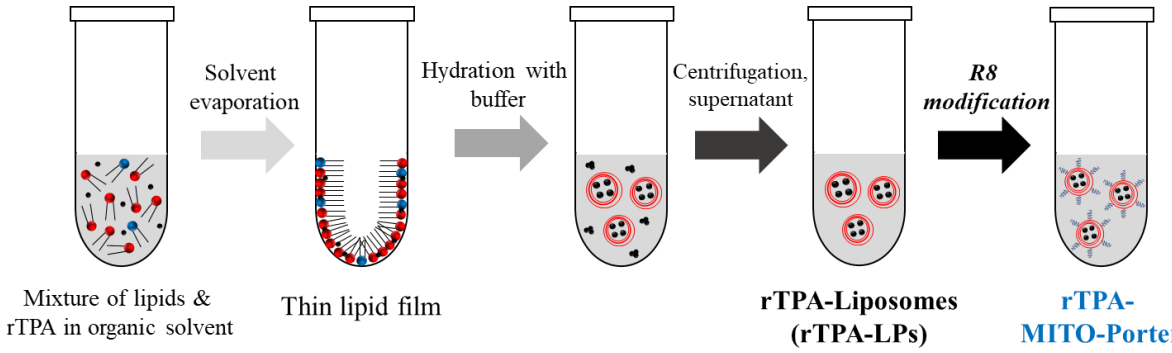

Figure 2-1 Schematic illustration of the preparation of the rTPA-MITO-Porter*. The total lipids' concentration of 0.55 mM with the initial rTPA concentration of 5 mol% was used in the preparation process using the hydration method.*

Table 2.1 Particle characteristics of the rTPA-encapsulated liposomal nanocarrier

Liposome type	Composition (molar ratio)	Diameter (nm)	Polydispersity index	ζ-potential (mV)	Encapsulation efficiency (%)
rTPA-LPs	DOPE:SM (9:2)	134 ± 3	0.24 ± 0.03	(-)24 ± 4	41 ± 7
rTPA-MITO-Porter	DOPE:SM-R8 (9:2-10 mol%)	157 ± 7	0.23 ± 0.02	(+)32 ± 3	41 ± 7
rTPA-EPC:SM-R8	EPC:SM-R8 (9:2-10 mol%)	163 ± 6	0.24 ± 0.02	(+)27 ± 2	44 ± 14

2.2.2 Photoinduced Singlet Oxygen Generation Ability

The ability of rTPA-loaded nanocarrier to produce singlet oxygen during the photoirradiation process was assessed using a singlet oxygen sensor green (SOSG) assay in a simple glass tube experiment. The SOSG reagent composes of the covalently linked of the fluorescein structure with the anthracene moiety. In the typical condition, the SOSG exhibits a weak fluorescence intensity due to the photoinduced electron transfer (PET) quenching effect within the anthracene and the fluorescein moiety. However, in the presence of singlet oxygen, the anthracene promptly reacts with singlet oxygen, following in the formation of endoperoxide accompanied by the loss of PET quenching effect on the fluorescein moiety (47). The increment on the fluorescence intensity of the solution at 530 nm correlates with the increase of the singlet oxygen level.

The rTPA in the nanocarrier system was mixed with the SOSG solution, and the alteration in fluorescence intensities of the SOSG was then recorded during the photoirradiation process using a Xenon lamp with an optical filter (700 ± 6 nm, 20 mW/cm^2). The same concentration of meso-tetra(4-sulfonatophenyl) phorphine, a commercially available porphyrin-based singlet oxygen photosensitizer, was used as a positive control with irradiation at 430 nm (20 mW/cm^2). As shown in **Figure 2-2**, the rTPA generates singlet oxygen in a comparable manner with the pristine porphyrin molecule. Furthermore, the singlet oxygen level increases linearly with longer irradiation time, indicating the stability of the rTPA compound

during the irradiation process. This result confirms the significant ability of the rTPA in generating singlet oxygen under NIR light irradiation.

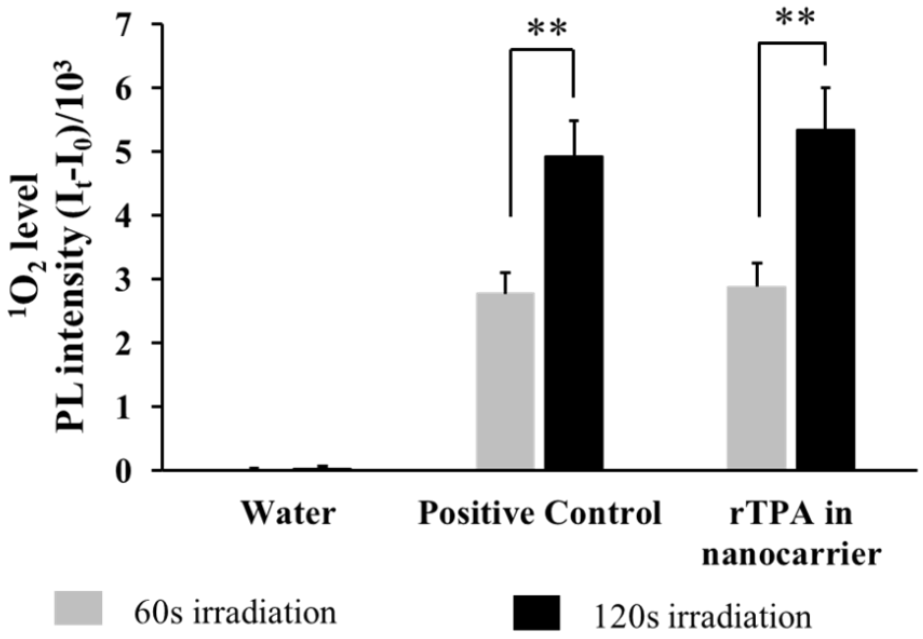

Figure 2-2 Photoinduced singlet oxygen generation ability evaluated by SOSG*. The rTPA in nanocarrier system was irradiated by 700 nm light (20 mW/cm^2), while the positive control (meso-tetra(4-sulfonatophenyl) porphin) illuminated by 430 nm light at the same light density. Error bars indicate S.D. (n = 3, **p<0.01 by paired T-test).*

The singlet oxygen generation ability of the rTPA-MITO-Porter was further evaluated using the Si-DMA probe. This probe composes of silicon-containing rhodamine and anthracene moieties that are predominantly accumulating in the mitochondria of living cells. The anthracene moiety has the function as the singlet oxygen reactive site, while the rhodamine serves as the fluorescence chromophore and mitochondria targeting moiety. This probe could be appropriated for recognizing the singlet oxygen level selectively in the mitochondrial compartment of living cells (48). As a result, the mitochondrial singlet oxygen level of HeLa cells was distinctly increased following the PDT process of the rTPA-MITO-Porter, while no alteration was observed in the cells treated by the rTPA-LPs (**Figure 2-3**). This result implies the potential ability of the rTPA-MITO-Porter to selectively induce the production of singlet oxygen in the mitochondria of tumors during long-wavelength light irradiation in addition to the selective mitochondrial accumulation of the rTPA compound delivered by the MITO-Porter system.

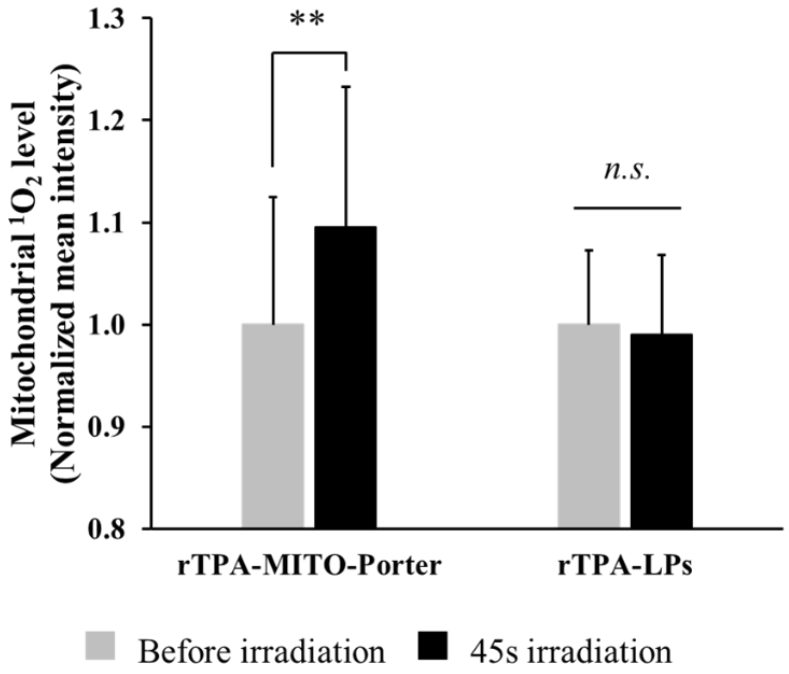

Figure 2-3 Mitochondrial singlet oxygen level detected by Si-DMA probe*. The fluorescence signal of the Si-DMA was detected using CLSM followed by the quantitative measurement of the intensity by ImageJ software. Data are represented as the mean with S.D. from 10 randomly-selected cells (n.s. = not significant; **p<0.01 by paired T-test).*

2.2.3 Detection of Mitochondrial Superoxide Level

It has been shown in the previous section that the rTPA-MITO-Porter has a robust capacity in producing a high level of singlet oxygen, selectively in the mitochondrial compartment of tumors, during a 700-nm light irradiation process. However, the additional investigation of different types of ROS, specifically superoxide ($O_2^{\bullet-}$) as the natural ROS produced mainly in mitochondria during the oxidative phosphorylation process, is required to evaluate the mitochondria oxidative level during the PDT process. The evaluation was carried out using MitoSOX^{TM} Red, a mitochondria-specific fluorogenic dye for detecting superoxide levels in mitochondria of living cells. The CLSM was employed to recognize the fluorescence signal of the MitoSOX^{TM} Red in the cells treated by free rTPA and several liposomal formulations of rTPA. In the absence of a light irradiation process, all treated cells displayed a negligible red fluorescence signal of the MitoSOX^{TM} Red. Nevertheless, after 3 minutes illumination of 700-nm light, the intense red fluorescence signal started to appear on the cells treated by the rTPA-MITO-Porter, while no fluorescence signal was detected on the other

control groups, as shown in **Figure 2-4**. This result indicates the increase of mitochondrial superoxide levels during the PDT process of the rTPA-MITO-Porter.

The increased level of mitochondrial superoxide may be occurred due to the oxidative damage of the mitochondrial electron transport chain (ETC) by singlet oxygen, which massively produced during the PDT process of the rTPA-MITO-Porter. This process may cause the release of electrons from the ETC that could react inadequately with the molecular oxygens to form the superoxide (27). This kind of phenomenon is also recognized as ROS-induced ROS release (49), in this case, singlet oxygen-induced superoxide release. Based on this result, it can be concluded that the rTPA-MITO-Porter not only exhibits an excellent ability to produce singlet oxygen but also can provoke the formation of the other ROS, such as superoxide in mitochondria which would strengthen the PDT effect even more.

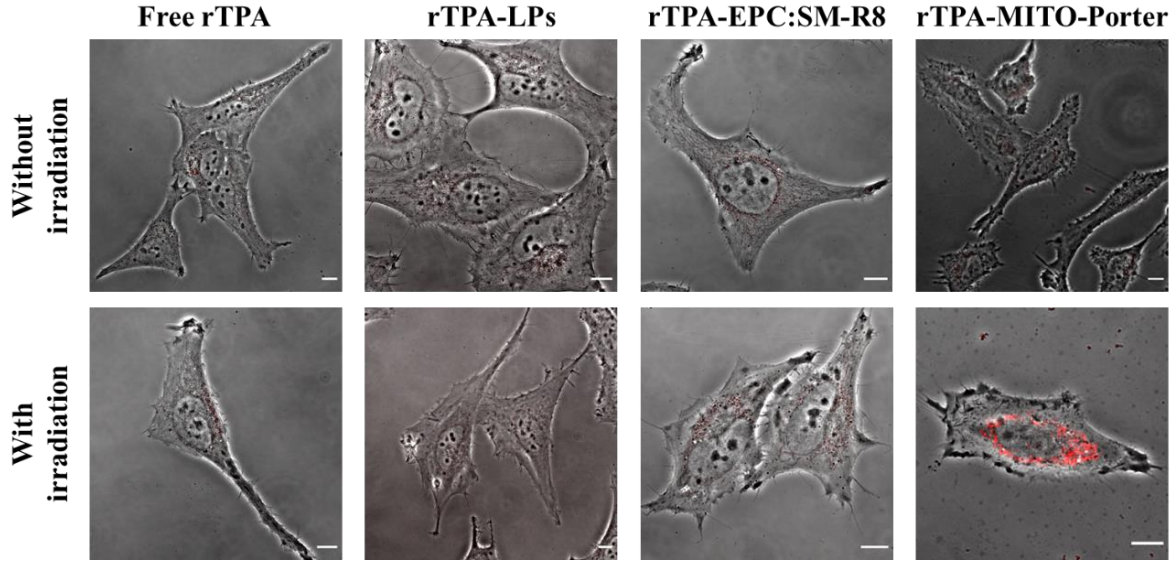

Figure 2-4 Mitochondrial $O_2^{\bullet-}$ level detected by MitoSOX™ Red. *The representative CLSM images of HeLa cells treated by free rTPA and several liposomal formulations of rTPA in the absence and presence of 3 minutes irradiation of 700-nm light. The appearance of the red fluorescence signals signifies the high level of superoxide in the mitochondrial compartment. Scale bars: 10 μm.*

2.2.4 Quantitative analysis of cellular uptake efficiency

Cell internalization is the first essential process for the organelle-selective delivery of photosensitizer. The nanocarrier system should have the ability to pass through the cellular membrane as the first barrier for the cellular internalization. The failure in the internalization process will have a significant impact on the further delivery process. Therefore, the quantitative analysis of the cellular uptake efficiency of the particles is one of the most important aspects to be studied. The quantification of cellular uptake efficiency was conducted using fluorescence-activated cell sorting (FACS) analysis. In this evaluation, I examined the cellular uptake of rTPA delivered by unmodified liposomes (rTPA-LPs), R8-modified liposomes (rTPA-MITO-Porter), and rTPA-EPC:SM-R8 in HeLa cells as the human malignant cells model. Every nanocarrier system was labeled by the NBD dye that could emit the green fluorescence signal. The cellular uptake efficiency was drastically increased up to 3.5 folds after the R8 modification either in the MITO-Porter system or the EPC:SM-R8 liposomes in comparison to the unmodified liposomes (**Figure 2-5**). Moreover, the cellular uptake efficiency of the rTPA-MITO-Porter and the rTPA-EPC:SM-R8 was found to be similar, indicating the same level of particle internalization. This result is consistent with previous reports (50,51) and indicates the critical roles of the R8 surface modification for magnifying the cellular uptake capability of the liposomal nanocarrier.

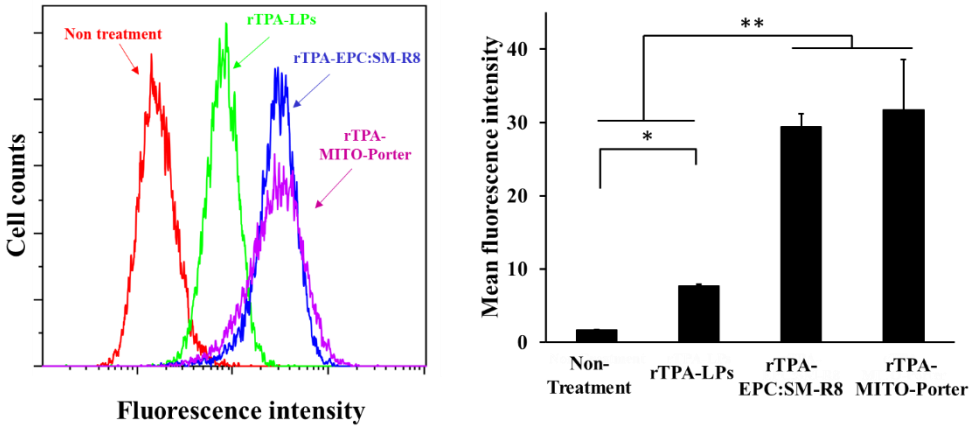

Figure 2-5 Cellular uptake efficiency*. The left graph represents the flow cytometry histogram of cellular uptake efficiency of several rTPA-loaded liposomal nanocarriers in HeLa cells. The mean fluorescence intensity (MFI) value indicates the level of particles taken up by the cells (right graph). Data are represented as the average MFI value with S.D. from a minimum of four independent experiments (*p<0.05; **p<0.01 by ANOVA followed by SNK-test).*

2.2.5 Intracellular Trafficking Profile

The next crucial intracellular event after cellular internalization is the intracellular trafficking process, followed by the accumulation of the particles in the target organelle. It was reported that the high density R8-modified liposomal nanocarriers are mainly internalized through macropinocytosis (35). Therefore, to reach the target organelle, the nanoparticles should have the endosomal escape ability to avoid lysosomal degradation. The intracellular trafficking profile of the rTPA-loaded nanocarriers was evaluated by CLSM. In this evaluation, the rTPA-liposomal nanocarriers were labeled with NBD dye, while the mitochondrial compartment was stained with MitoTracker^{TM} Deep Red FM. The cells were treated by the rTPA-LPs, rTPA-EPC:SM-R8, and rTPA-MITO-Porter for 1 h in the serum-free medium followed by 2 h incubation in the medium containing serum. The first 1 h incubation aims to facilitate the cellular internalization process of the particles, while the next 2 h incubation is required for the endosomal escape and mitochondrial accumulation process. In the case of rTPA delivered by unmodified liposomal nanocarrier, there was no green fluorescence signal of the nanoparticle could be detected. It indicates the low or negligible amount of the nanoparticles inside the cells due to the low cellular uptake efficiency, as it has been shown on the cellular uptake efficiency study.

Interestingly, the rTPA-EPC:SM-R8, which has a similar cellular uptake efficiency in comparison to the rTPA-MITO-Porter, displayed a distinct intracellular trafficking manner. Most of the rTPA-EPC:SM-R8 accumulated outside the mitochondria compartment of HeLa cells, indicated by the separation of the green fluorescence signal of the nanoparticles and the red fluorescence signal of the mitochondria. In contrast, the rTPA-MITO-Porter dominantly concentrated in the mitochondria, indicated by the appearance of several yellow signals that are produced by the overlapping of the green and red fluorescence signals of the nanoparticles and mitochondria, respectively (**Figure 2-6**). All the results mentioned above suggest that the important role of DOPE and R8 moieties for the mitochondrial delivery of the MITO-Porter system.

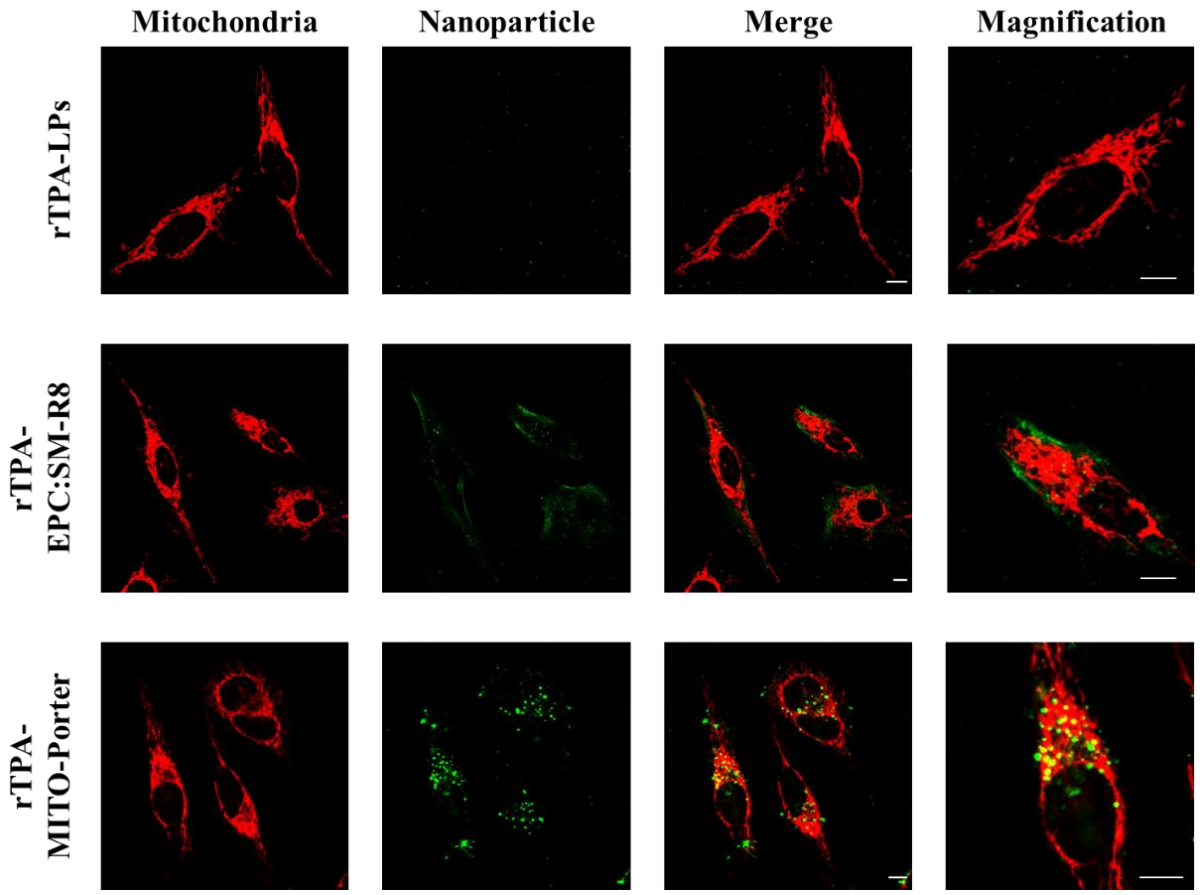

Figure 2-6 The intracellular trafficking profile. *The representative CLSM images of the intracellular trafficking profile of several rTPA-loaded liposomal nanocarrier systems in HeLa cells. The mitochondrial compartment was stained by MitoTracker™ Deep Red FM, while the nanocarrier was labeled by NBD dye. The yellow signals represent the colocalization of nanoparticles in mitochondrial compartment. Scale bars: 10 μm.*

The mitochondrial accumulation level was then quantified by calculating Pearson's correlation coefficient (PCC) of several randomly-selected CLSM images by using ImageJ software (52). In general, the PCC has the value ranges from -1 to +1. The -1 value indicates a negative correlation, while the 0 value and +1 value mean no correlation and the perfect correlation between two objects, respectively (53). From the PCC value, the rTPA-MITO-Porter showed the highest colocalization degree as opposed to the rTPA-LPs and rTPA-EPC:SM-R8 (**Figure 2-7**). This result further validates the efficiency of the MITO-Porter system in delivering the rTPA compound selectively into the mitochondrial compartment.

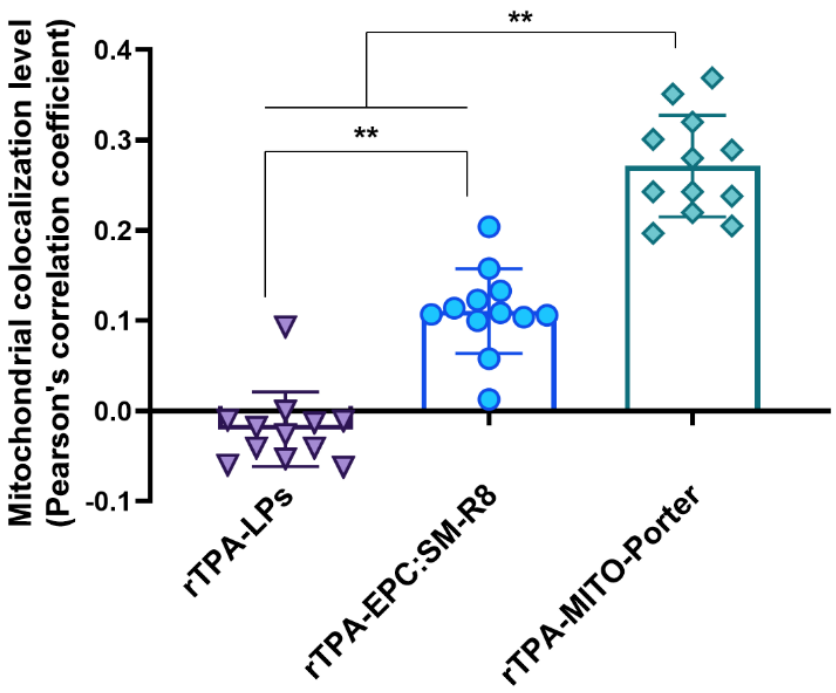

Figure 2-7 Mitochondrial colocalization level. *Pearson's correlation coefficient (PCC) was calculated using ImageJ software from several randomly-selected CLSM images. Error bars indicate S.D. (n = 12, **p<0.01 by ANOVA followed by SNK-test).*

To further verify the mitochondrial accumulation of rTPA, the direct observation of the rTPA signal in the mitochondria was conducted by the utilization of a highly sensitive CLSM system (A1Rsi and Ti-E, Nikon Corporation; Tokyo, Japan). This kind of CLSM system is required to detect a weak fluorescence signal of rTPA, which cannot be detected by the standard CLSM system. In this evaluation, I made a comparison of the mitochondrial accumulation of free rTPA, rTPA-LPs, rTPA-EPC:SM-R8, and rTPA-MITO-Porter in HeLa cells. The mitochondrial compartment was stained using MitoTracker Orange CM-H2TMRos (Thermo Fischer Scientific Inc.). As shown in **Figure 2-8**, the rTPA signal could be detected in different levels of intensity depending on the delivery system. The rTPA delivered by the MITO-Porter system exhibited the most robust signal inside the cells, while a low level of fluorescence was observed for the rTPA-LPs and the rTPA-EPC:SM-R8. Besides, there was no fluorescence signal could be detected for the cells treated by the free rTPA.

Furthermore, some of the rTPA signals colocalized with the mitochondrial compartment of the cells treated by the rTPA-MITO-Porter indicated with the appearance of some yellow signals. In contrast, a negligible colocalization signal was observed in the case of other rTPA formulations. These results further provide stronger evidence regarding the effectivity of the

MITO-Porter system in transporting the rTPA compound selectively into the mitochondrial compartment of tumor cells.

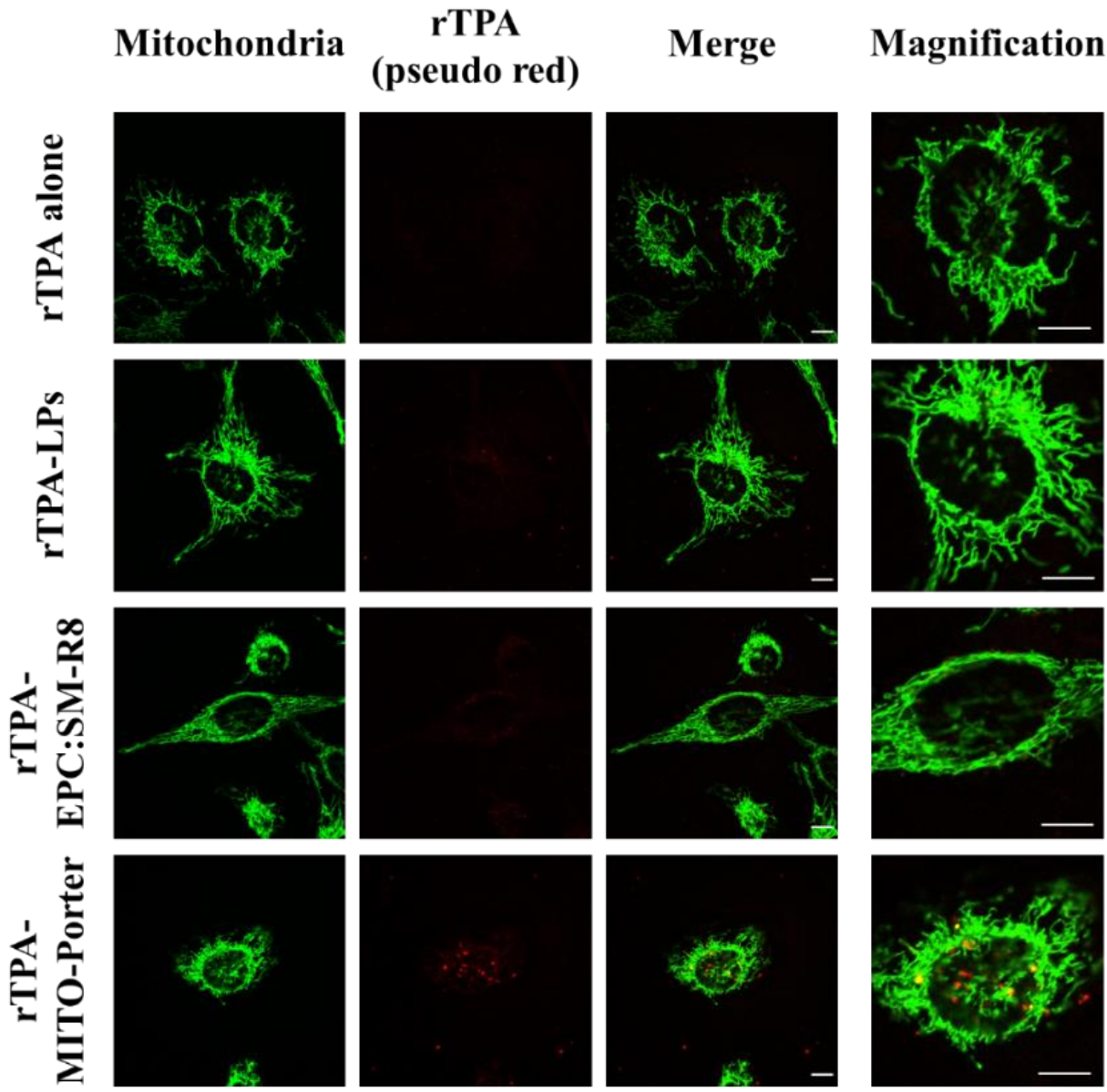

Figure 2-8 Mitochondrial accumulation of rTPA. *The representative CLSM images of HeLa cells treated by several rTPA formulations. Mitochondrial compartment was stained with MitoTracker Orange CM-H2TMRos. The yellow spot is represented the colocalization of rTPA in mitochondrial compartment. Scale bars: 10 μm.*

2.2.6 Evaluation of *in vitro* PDT toxicity

After validating the physical characteristics, photophysical properties, and biological behavior of the rTPA-MITO-Porter, the investigation was proceeded by evaluating the PDT concept and its effectivity to annihilate human cancer cell lines. The PDT effectivity was evaluated by comparing the cytotoxicity profile of the rTPA-MITO-Porter with the other rTPA formulations against HeLa cells, as the human cancer cell line model. The cytotoxic effects were determined using a colorimetric method that is a WST-1 assay in the absence and presence of a light irradiation process. In this evaluation, the cells were treated by several rTPA formulations for 1 h in the serum-free medium, followed by 2 h incubation using a medium containing 10% FBS. This incubation time was previously validated to be effective for mitochondrial delivery, as explained in the intracellular trafficking profile. In the case of cells treated by free rTPA and rTPA-LPs, negligible toxicity was observed either in the absence or in the presence of a light irradiation process (**Figure 2-9**). These results could be explained by the poor cellular uptake efficiency of both free rTPA and rTPA-LPs. Furthermore, a 3-minute irradiation process using Xenon lamp with a light density of 68.5 mW/cm^2 could not induce significant toxicity toward the cells, which is a crucial issue to be considered as the safety aspects of phototherapy.

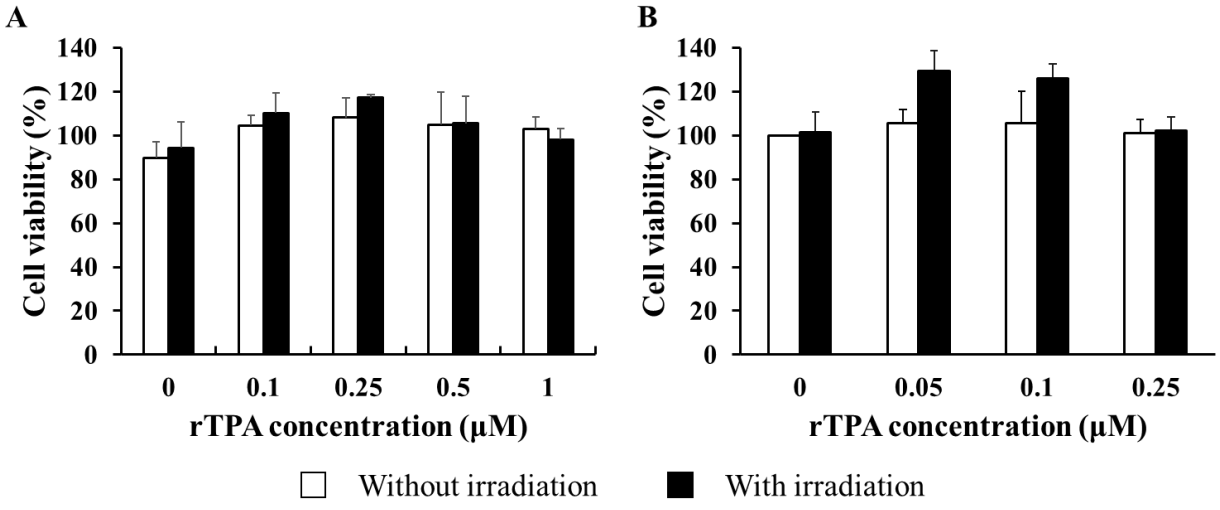

Figure 2-9 PDT cytotoxicity of free rTPA and rTPA-LPs against HeLa cells*. A. free rTPA; B. rTPA-LPs, evaluated in the absence and presence of light irradiation (Xenon lamp at 700 ± 6 nm; 68.5 mW/cm^2). Data represent as average with S.D. from three independent experiments.*

The evaluation of the PDT cytotoxicity was continued by treating the cells with the rTPA-EPC:SM-R8, as a non-mitochondrial targeting system. Based on the cellular uptake and intracellular trafficking study, this particle could efficiently be internalized by the HeLa cells, with the limited mitochondrial accumulation. From the WST-1 assay, more than 90% of the cell population remained intact after treatment in the range of rTPA concentrations tested both in the absence and presence of a light irradiation process (**Figure 2-10**). This result indicates that only the internalization of the rTPA is not sufficient to induce significant cytotoxicity.

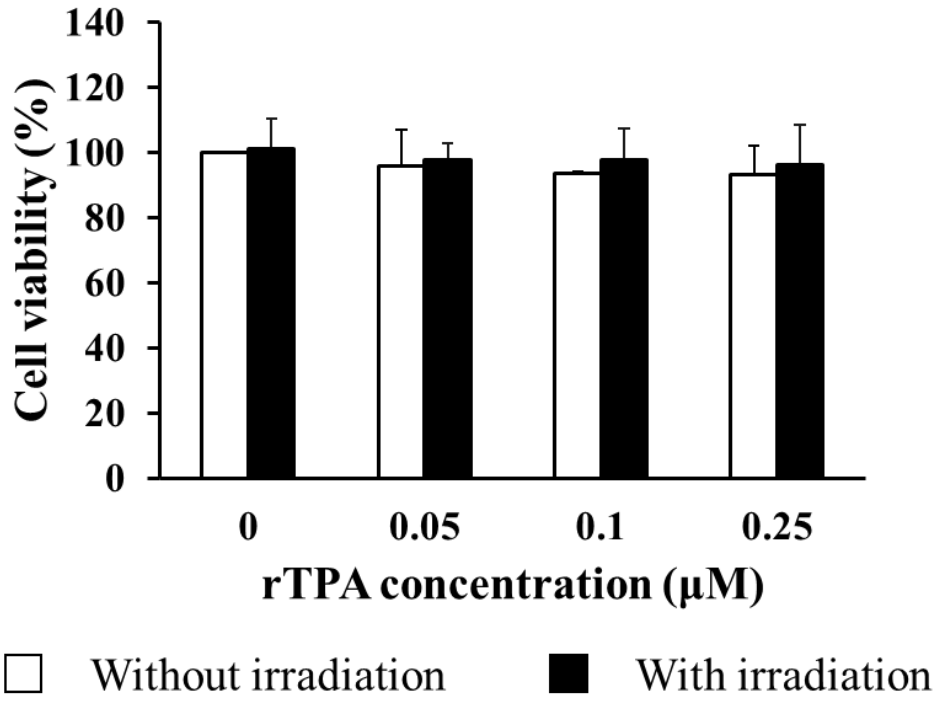

Figure 2-10 PDT cytotoxicity of rTPA-EPC:SM-R8 againts HeLa cells*. The evaluation was performed in the absence and presence of light irradiation (Xenon lamp at 700 ± 6 nm; 68.5 mW/cm^2). Value = mean ± S.D. (n = 3).*

Notable toxicity was observed when the rTPA-MITO-Porter combined with 3 minutes irradiation of 700-nm light with the same light density was applied into the HeLa cells. Furthermore, a dose-dependent toxicity profile was obtained with the minimum required concentration for eliminating half of the cell population (EC_{50}) approximately 0.16 ± 0.02 μM. In contrast, there was no significant toxicity during the rTPA-MITO-Porter treatment in the absence of a light irradiation process (**Figure 2-11**). This result implies several essential points regarding the utilization of the rTPA-MITO-Porter for PDT application. First, the rTPA-MITO-Porter is a safe system for the cells in the absence of a light irradiation process. Second, the 700-nm light is suitable to activate the rTPA-MITO-Porter to induce cellular damage, which is an advantage for the PDT application. Finally, the utilization of the MITO-Porter system as a carrier for rTPA could maximize the PDT cell-killing ability of the rTPA compound.

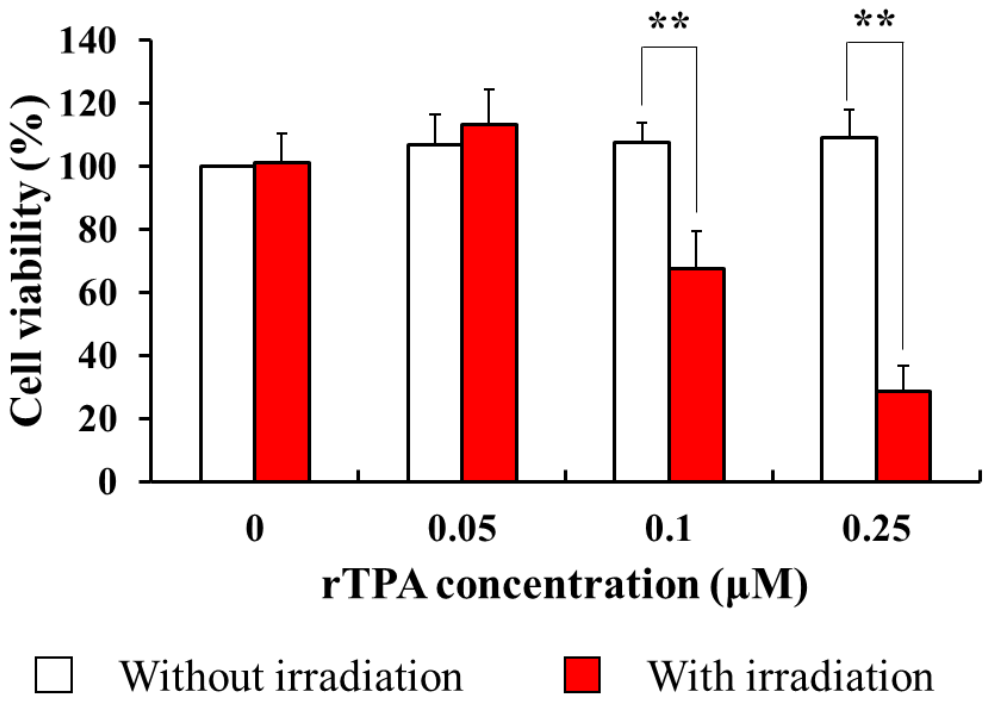

Figure 2-11 PDT cytotoxicity of rTPA-MITO-Porter against HeLa cells*. The irradiation process was performed using a Xenon lamp with the optical filter for producing 700 ± 6 nm with a density of 68.5 mW/cm^2. Data represent the average value of cell viability with S.D. (n =3; **p<0.01 by unpaired T-test).*

The PDT cytotoxicity of the rTPA-MITO-Porter was further evaluated against another type of human cancer cell line, namely SAS cell. This type of malignant cell is derived from a human tongue cancer cell. This cell is considered as a potential target for PDT due to its fatality and cell location on the surface of the body that can be easily treated by PDT. As shown in **Figure 2-12**, there was no significant toxicity of the rTPA-MITO-Porter in the absence of light irradiation. In contrast, after applying 5 minutes of light illumination (700 ± 6 nm, 68.5 mW/cm^2), the cell viability was significantly reduced with the EC_{50} value of 0.41 ± 0.18 μM. This result confirms the universality of the rTPA-MITO-Porter for PDT applications, which could be used to eradicate different types of human cancer cell lines.

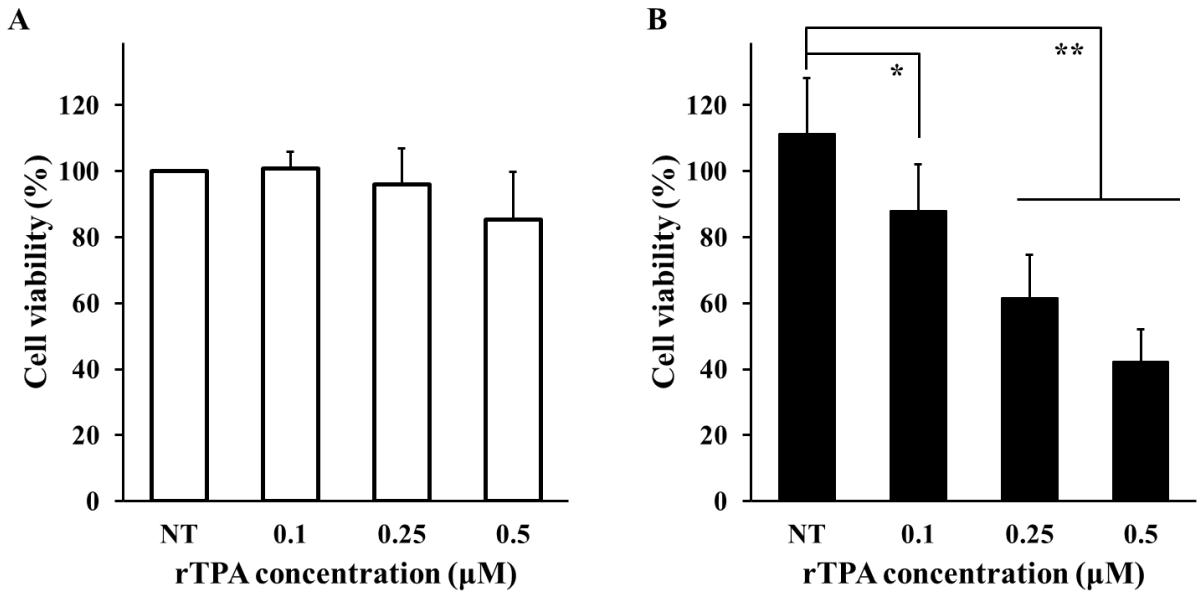

Figure 2-12 PDT cytotoxicity of rTPA-MITO-Porter against SAS cells*. A. in the absence of light irradiation; B. in the presence 5 minutes light irradiation at 700 ± 6 nm (68.5 mW/cm^2). Error bars indicate S.D. (n = 4; *p<0.05; **p<0.01 by ANOVA followed by Dunnett test).*

2.2.7 Validation of Mitochondria as the Important Target for PDT

The significance of mitochondria delivery of rTPA was validated by comparing the cell-killing ability of the mitochondrial delivery system of the rTPA-MITO-Porter with the non-mitochondria targeting system of the rTPA-EPC:SM-R8. This comparison was made based on the findings that both liposomal systems could be efficiently internalized by the cells at the same level, with a significant difference in the mitochondrial accumulation level. The comparison was conducted using the same concentration of rTPA (0.25 μM), either in the absence or presence of 3 minutes light irradiation process. As a result, both systems are safe for the cells in the absence of light irradiation process, as indicated by negligible toxicity. During the PDT process, only the rTPA-MITO-Porter could induce significant toxicity against HeLa cells, with more than 70% of the cell population was being killed. This result suggests that the importance of mitochondria as the PDT target. Furthermore, the combination of the light irradiation process and mitochondrial delivery of rTPA is required to induce remarkable cytotoxicity (**Figure 2-13**).

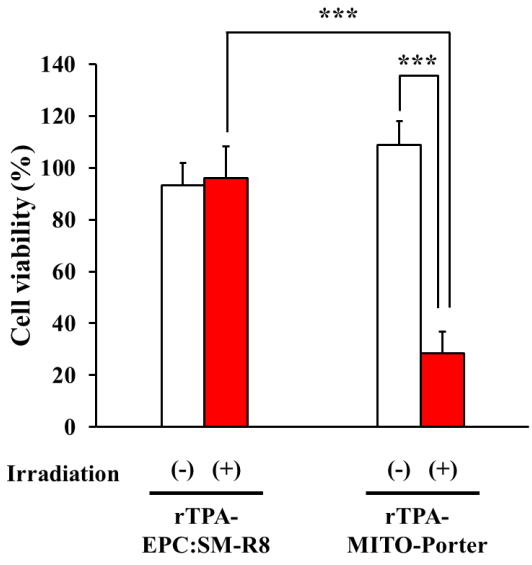

Factor	P-value
Irradiation	<0.001
Mitochondria delivery	<0.001
Interaction between irradiation and mitochondria delivery	<0.001

Figure 2-13 Validation of mitochondria as the potential target for PDT*. The two-way ANOVA analysis was performed to investigate the effect of irradiation and mitochondria delivery of rTPA on the cytotoxicity against HeLa cells. The significant differences between each treatment conditions are calculated by a simple main effect test followed by Bonferroni correction (***p<0.001). Value = mean ± S.D. (n = 3).*

2.2.8 Validation of cell death mechanism

Several cell death mechanisms, including apoptosis (54), necrosis (55), and autophagy (56), could be activated during the PDT process. The variation of the cell response to the PDT depends on the cell type or its genetic or metabolic status, the types of photosensitizers, and the total light dose (57). Furthermore, the subcellular accumulation of the photosensitizer in the specific organelle also plays an essential role in determining the PDT cell death mechanism. For instance, the mitochondrial accumulation of photosensitizer could effectively induce the activation of the apoptosis pathway, while the plasma membrane localization may initiate the necrotic cell death (58,59).

The cell death mechanism during the PDT process of the rTPA-MITO-Porter was validated by obtaining the alteration of the cell morphology during the irradiation process using CLSM live-imaging observations. As shown in **Figure 2-14**, the cell experienced shrinkage into a smaller size without losing the integrity of the plasma membrane. Furthermore, the formation of membrane blebs was observed, followed by the generation of rounded-shape apoptotic bodies at the end of the irradiation process. A significant alteration on the mitochondria structure was also observed. Before starting the irradiation process, the mitochondria structure displayed a vast interconnected network with a filamentous structure. It indicates the sound condition of mitochondria. However, during the irradiation process, the mitochondria structure became fragmented, resulting in the small dot-like structures, indicative of the damage of the mitochondria network. All those characteristics are consistent with the specific hallmarks of the apoptosis process (60,61). In contrast, there was no significant alteration either in the cell membrane structure or in the mitochondrial compartment condition of the cells treated by the rTPA-LPs. These results suggest that the PDT cytotoxic effect of the rTPA-MITO-Porter is through the activation of the apoptotic pathway.

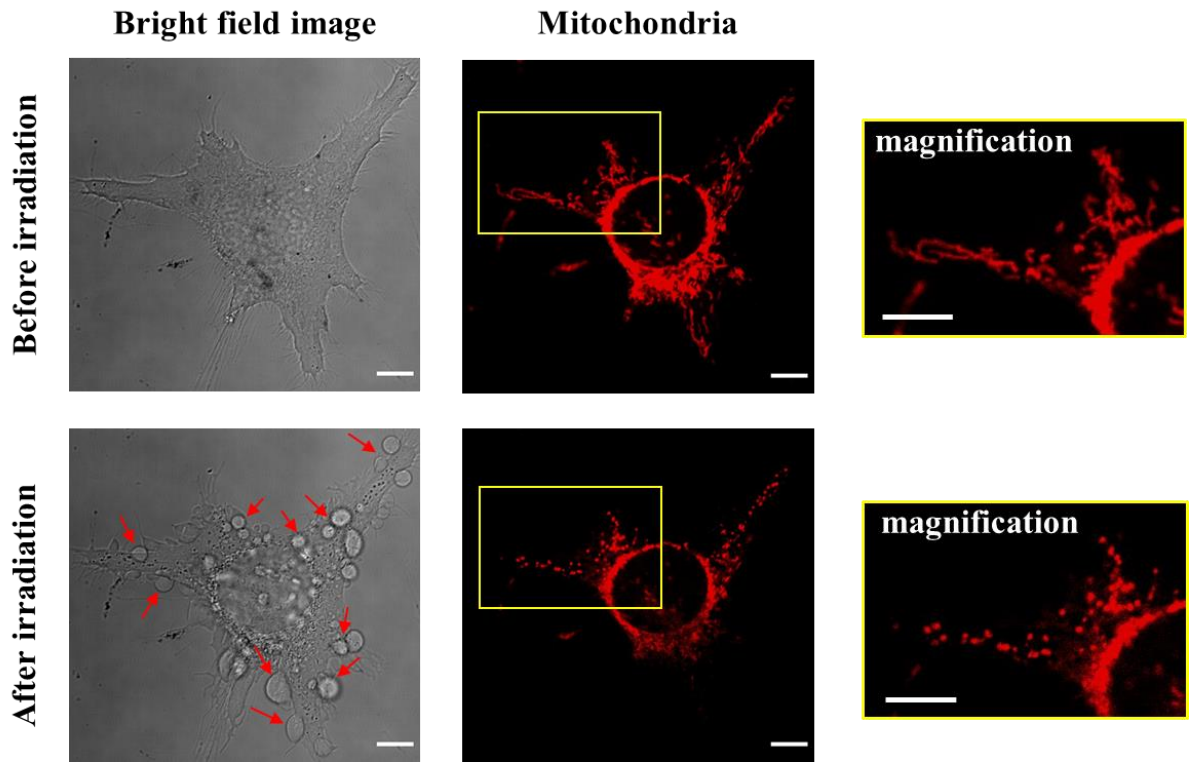

Figure 2-14 The alteration on the cell morphology. *The representative image of HeLa cells treated using rTPA-MITO-Porter, before and after the light irradiation process, captured by the live-imaging CLSM system. The bright-field image represents the alteration of the plasma membrane structure. The red arrows indicate the formation of membrane bleb. Scale bars: 10 μm.*

2.3 Discussion

The PDT effect is a resultant from the dynamic interaction between its key elements, specifically photosensitizer, light, and oxygen molecules. The energy transfer process from the harmless visible light, as the source of energy, to the molecular oxygen mediated by the photosensitizer, resulting in the alteration of the typical oxygen molecule to the highly reactive and harmful species, mainly singlet oxygen. However, singlet oxygen has a short lifetime and limited diffusion capacity, creating the limitation of the harmful effect on the cells. Moreover, the lack of oxygen concentration in some solid tumors (hypoxia) is one of the most challenging problems in the PDT application. It was reported that the inhibition of the mitochondrial respiration, either by the chemicals or PDT process, causes the increment of oxygen concentration in mitochondria (28,31), which could be an advantage for the PDT process, particularly in the hypoxic condition. Furthermore, the increased level of ROS specific inside the mitochondrial compartment causes depolarization of the mitochondrial membrane, leading to the release of the proapoptotic factor such as cytochrome c from the mitochondria to the cytosol, followed by the activation of caspase pathway to start the apoptosis process (30,62,63). By selective delivery of photosensitizer into the mitochondrial compartment, the harmful effect of ROS could be concentrated in the mitochondria, and it could be one advantage of the mitochondria selective targeting PDT system to obtain the full benefits of PDT.

The incorporation of the rTPA compound into the MITO-Porter system has been achieved by using the hydration method. The MITO-Porter system was constructed by the combination of DOPE and SM lipids with the molar ratio of 9:2 and surface modification with an arginine-rich cell-penetrating peptide of R8. The resulting particles displayed homogenous particle distribution with an average particle diameter of 157 ± 7 nm. The particle size was comparable when the DOPE lipid was replaced by the EPC lipid to produce the non-mitochondrial targeting particles, namely the rTPA-EPC:SM-R8. Both particles also exhibited a highly positively-charged characteristic, due to the attachment of R8 on the exterior of the particles. Furthermore, the rTPA in negatively-charged liposome containing DOPE and SM without R8 modification was also prepared as the control particle.

The rTPA in the nanocarrier system readily generated a high level of singlet oxygen during the photoirradiation process using a 700-nm light system and comparable with the pristine porphyrin structure, which required a shorter wavelength of light (430 nm) for the activation process. Furthermore, the mitochondrial delivery of the rTPA compound by the MITO-Porter system exhibited an active singlet oxygen production profile in HeLa cells. The

massive production of singlet oxygen in the mitochondrial compartment further produced a significant impact on the mitochondrial ETC, indicated by the increase of superoxide levels during the PDT process. Superoxide is a natural by-product during the mitochondrial oxidative phosphorylation process. The electron escape during this transport process leads to the production of superoxide through the inappropriate reaction with the oxygen molecules. In the typical condition, cells have a defense mechanism to eliminate this ROS and control its level on the safe concentration for the cells. Therefore, the increased level of superoxide during the PDT process of the rTPA-MITO-Porter could be a sign of the damage to the mitochondrial ETC.

The attachment of R8 moieties on the surface of the particles exhibited a notable increment on the cellular uptake efficiency of the rTPA-MITO-Porter and the rTPA-EPC:SM-R8, while unmodified liposomes (rTPA-LPs) displayed an ineffective cell internalization profile. R8 is one of the most popular arginine-rich cell-penetrating peptides (CPPs) that extensively used to intensify the cell internalization of the nanoparticles. The arginine-rich CPPs could activate the macropinocytosis pathway by the interaction with the cell-surface proteoglycans (64). R8 also demonstrated an efficient endosomal escape *via* membrane fusion with the endosomal membrane at both neutral (early endosome) and acidic (late endosome) environment, which can protect the liposomes from the lysosomal-degradation (65). Though the cellular uptake efficiency between the rTPA-MITO-Porter and the rTPA-EPC:SM-R8 was similar, the intracellular trafficking of both liposomal systems was different, particularly in the mitochondrial accumulation level. Most of the rTPA-EPC:SM-R8 particles failed to reach the mitochondrial compartment, while the rTPA-MITO-Porter was dominantly concentrated in the mitochondria. The lack of mitochondrial accumulation level of the rTPA-EPC:SM-R8 could be associated with the presence of EPC as a substituted-lipid of DOPE. It was reported that the EPC lipid could reduce the endosomal escape ability of the cationic liposomal nanocarrier, regardless of the presence of R8 moieties (33,66). Thus, most of the rTPA-EPC:SM-R8 entrapped inside the endosome during the internalization process.

The distinction in the intracellular trafficking profile and mitochondrial accumulation level resulted in a great impact on the PDT cytotoxicity of the rTPA compound (**Figure 2-15**). The low cellular uptake efficiency and negligible mitochondrial accumulation of the free rTPA and the rTPA-LPs could be linked to the negligible toxicity against HeLa cells. Additionally, the free rTPA has highly hydrophobic characteristics, which may cause the aggregation, especially in the aqueous solution. The aggregation causes a reduction in the light absorption capacity and increases the probability of rapid deactivation of the photoexcited state of the

sensitizer molecule (39). Both would drive to the suppression of the singlet oxygen generation (67).

Furthermore, when the rTPA compound was delivered by the EPC:SM-R8 system, negligible toxicity was obtained either in the absence or in the presence of a light irradiation process. Whereas, a massive cell killing process was observed in the cells treated by the rTPA-MITO-Porter in combination with a 700-nm light irradiation process. This result could be associated with the specific localization of the photochemical reaction on the mitochondrial compartment of tumors. Furthermore, the utilization of the MITO-Porter system for transporting the rTPA compound resulted in a robust cell-killing ability against two different types of human cancer cell lines, specially HeLa cell and SAS cell, indicated by the relatively low EC_{50} value compared to several reported PDT systems, as shown in **Table 2.2**. Also, the activation of the apoptosis cell death was found to be intensive during the PDT process of the rTPA-MITO-Porter. These results suggest that the synergistic combination effect of the rTPA and the MITO-Porter system is required to obtain the full PDT benefits of the rTPA compound. Furthermore, the mitochondrial delivery of the rTPA compound by the MITO-Porter system is the key factor for enhancing the PDT effectivity, indicating the importance of mitochondria as the potential target for PDT.

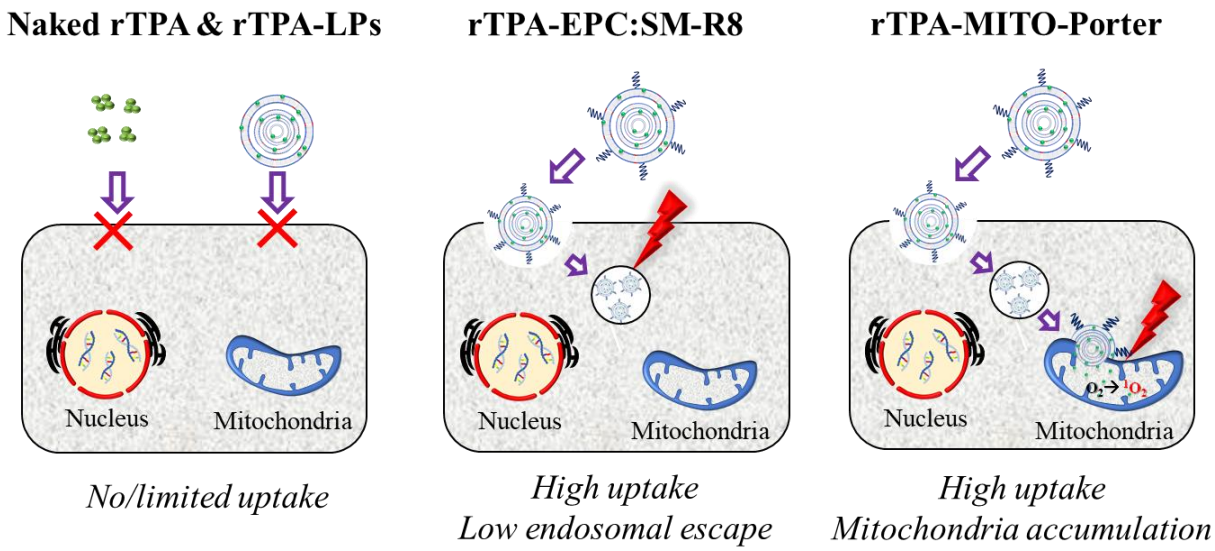

***Figure 2-15 Illustration of the biological behavior of several rTPA formulations**. The distinction in the cellular uptake, intracellular trafficking, and mitochondrial delivery of rTPA significantly affect the PDT effectivity.*

Table 2.2 Comparison of PDT effectivity

Compound-system name	Irradiation condition	Cells	EC_{50}*	Ref.
rTPA-MITO-Porter‡	700 nm; 12.4 J/cm^2	HeLa	0.16 μM (0.26 μg/mL)	*This work*
rTPA-MITO-Porter‡	700 nm; 20.6 J/cm^2	SAS	0.41 μM (0.64 μg/mL)	*This work*
Cationic octahedral molybdenum complex‡	460 nm; 18 J/cm^2	HeLa	0.1 μM	(68)
Pheophorbide-A‡	610 nm; 84 J/cm^2	MES-SA	0.5 μM	(69)
Heterometallic Ru-Pt metallacycle‡	450 nm; 6.54 J/cm^2	A549	0.71 μM	(70)
Chlorin conjugated with galactodendritic‡	>500 nm; 6 J/cm^2	UM-UC-3	1.3 μM	(71)
HA-IR-Pyr‡	808 nm; 37 J/cm^2	HeLa & MDA-MB-231	5-7 μM	(72)
Graphene quantum dot‡	980 nm; 720 J/cm^2	4T1	~80 μg/mL	(73)
Silicon phthalocyanine derivative	670 nm; 36 J/cm^2	A2780/AD	0.9 μg/mL	(74)
Protoporphyrin IX	>570 nm; 11.2 J/cm^2	HeLa	0.8 μM	(75)
Tetra(3,4-pyrido)-porphyrazines	>570 nm; 11.2 J/cm^2	HeLa	0.26 μM	(76)
Ru(II)polypyridyl complexes	450 nm; 12 J/cm^2	HeLa	3.5 μM	(77)
Octasulfonate-modified zinc (II) phthalocyanine	>610 nm; 27 J/cm^2	HepG2	3.78 μM	(78)
Photofrin®	>610 nm; 48 J/cm^2	HT29	5 μg/mL	
Meso-substituted porphyrin	650 nm; 24 J/cm^2	HeLa	5 μM	(79)
Porphyrin-ferrocene conjugate	620 nm; 21.6 J/cm^2	MCF-7	25 μM	(80)

*EC_{50}: minimum concentration that required to eliminate half of cell population;

‡Mitochondrial targeting system.

2.4 Summary and Conclusion

The novel mitochondrial targeting PDT system, namely the rTPA-MITO-Porter system, was successfully developed by combining a novel π-extended porphyrin-type photosensitizer, namely rTPA, with a MITO-Porter system, a versatile mitochondrial targeting liposomal-based nanocarrier. The synergistic action of this combination exhibited effective photoinduced cytotoxicity against two types of human cancer cell lines, specifically HeLa cell and SAS cell, with a relatively low EC_{50} value of 0.16 ± 0.02 μM and 0.41 ± 0.18 μM, respectively. The PDT process of the rTPA-MITO-Porter could effectively induce the activation of apoptosis cell death, which is preferable for cancer therapy due to the negligible inflammation effects, leading to minimum side effects for healthy cells. The results presented in this chapter provided an excellent opportunity for the subsequent utilization of the rTPA-MITO-Porter as a novel biologically-active nanomaterial for mitochondrial targeting PDT in the *in vivo* experiment.

CHAPTER 3

PDT Application on the Human Tumor Xenograft Mouse

CHAPTER 3
PDT APPLICATION ON THE HUMAN TUMOR XENOGRAFT MOUSE

After obtaining a promising PDT killing capacity of the rTPA-MITO-Porter, the investigation was continued into the translation process from the *in vitro* concept to the *in vivo* application. Before conducting the *in vivo* antitumor evaluation, several issues should be solved, particularly regarding the suitability between the amount of encapsulated drug inside the nanocarrier system with the required administration dose. Furthermore, for achieving the mitochondrial compartment of the tumor cells, the particle should have functional integrity during the transportation process throughout the tumor microenvironment, to protect the carried-drugs from the release and degradation. Therefore, further formulation design is required for the translation process of this novel mitochondrial targeting PDT system into the *in vivo* application.

This formulation design aims to achieve a suitable dose of administration of the rTPA and to have better particle integrity for an *in vivo* environment without affecting the mitochondrial delivery and its phototoxicity. Based on the cellular uptake and intracellular trafficking results in Chapter 2, it was found that the combination of DOPE and R8 moieties is the main factor that contributed to the mitochondrial delivery of MITO-Porter system. It is also reinforced by previously published paper regarding the analysis of mitochondrial delivery of the MITO-Porter system. It suggested that the alteration of the helper lipids, such as SM, cholesteryl hemisuccinate (CHEMS), cholesterol (Chol), and phosphatidic acid, did not significantly affect the mitochondrial accumulation level, as far as the DOPE and R8 are the main components of the MITO-Porter (36). Furthermore, it was reported that the presence of Chol in the liposomal formulation could increase the packing of phospholipid molecules, resulting in a more rigid and stable liposomal structure (81,82). Based on the reasons mentioned above, I attempted to design a better and suitable rTPA-MITO-Porter system by replacing the SM with Chol.

This chapter covers the translation process from the *in vitro* concept into the *in vivo* application of the rTPA-MITO-Porter system to treat human tumor cells xenografted on the mouse model. Before conducting the *in vivo* therapeutic activity evaluation, several adjustment processes on the rTPA-MITO-Porter formulation was implemented to achieve more desirable particle characteristics for the *in vivo* application. This formulation design process resulted in

a negligible alteration on the mitochondrial targeting ability and the phototoxicity profile. Furthermore, the antitumor activity was evaluated using a model mouse bearing SAS cells, human tongue cancer cells by monitoring the change of the tumor volume and body weight for 14 days. The mitochondrial membrane potential was also reported to evaluate the PDT effect on the tumor mitochondria.

3.1 Experimental procedures

3.1.1 Materials

The lipid materials consisting of 1,2-Dioleoyl-sn-glycero-3-phosphatidyl ethanolamine (DOPE) and cholesterol (Chol) were purchased from Avanti Polar Lipids, Inc. (Alabaster, AL, USA) and Sigma Aldrich Corp. (St. Louis, MO, USA), respectively. The MitoProbe^{TM} TMRM assay kit was obtained from Thermo Fischer Scientific Inc. (Waltham, MA, USA). SAS cells, human squamous cells carcinoma of the tongue, were supplied from National Institutes of Biomedical Innovation, Health, and Nutrition JCRB Cell Bank (Osaka, Japan). The cells were cultured in Dulbecco's Modified Eagle's Medium (DMEM) (Wako; Osaka, Japan) containing 10% (v/v) fetal bovine serum (FBS) (Sigma Aldrich Corp.) and penicillin-streptomycin (Meiji Seika Pharma, Co. Ltd.; Tokyo, Japan) under an atmosphere condition of 5% CO2/air at 37°C. The rTPA compound was synthesized by Yuta Takano, Ph.D. All additional chemicals and solvents used were purchased as commercially available reagent-grade products.

3.1.2 Preparation of the High Lipid Content rTPA-MITO-Porter

The rTPA-MITO-Porter was prepared using the hydration method, as explained before in the Chapter 2 with slight modification. Briefly, a combination of DOPE and Chol with the molar ratio of 9:2 and total lipids' concentration of 2.75 mM in ethanol solution was mixed with 5 mol% of rTPA in chloroform followed by solvent evaporation. The hydration process of the lipid film was carried out using 10 mM HEPES buffer containing 290 mM glucose (pH 7.4) for 15 minutes at room temperature; then sonication to form spherical-shaped and homogenous particles. The non-encapsulated drugs were removed by centrifugation at 20,600 x g for 5 minutes. Finally, the liposomes were modified with 10 mol% of R8 solution to obtain the rTPA-MITO-Porter. The particle size and zeta potentials were analyzed using dynamic light scattering (DLS) method and the patented technique of phase analysis light scattering

(M3-PALS technology), respectively. Moreover, the amount of encapsulated rTPA was determined using spectrophotometry.

3.1.3 Performance Verification of the High Lipid Content rTPA-MITO-Porter

The mitochondrial delivery ability was evaluated using CLSM analysis. SAS cells were seeded on a 35-mm glass base dish with a density of $2x10^5$ cells and incubated for 24 h. The NBD-labeled rTPA-MITO-Porter was added into the cells in serum-free medium for 1 h, followed by an additional 2 h in medium containing 10% serum. After completing the transfection process, the mitochondrial compartment was stained using 0.1 μM MitoTracker™ Deep Red FM for 20 minutes. The observation was performed by Olympus FV10i-LIV equipped with a water-immersion objective lens (UPlanSApo 60x/NA. 1.2) and a dichroic mirror (DM405/473/559/635). The NBD-labeled rTPA-MITO-Porter and the MitoTracker™ Deep Red FM were excited with 473 nm and 635 nm light, respectively. Two fluorescence detection channels were set using a filter at a bandpass of 490-540 nm to detect NBD-labeled rTPA-MITO-Porter and 660-710 nm to detect MitoTracker™ Deep Red FM.

The *in vitro* PDT cytotoxicity against SAS cells was evaluated by transfecting the cells with the rTPA-MITO-Porter for 1 h in serum-free DMEM, followed by 2 h incubation in DMEM containing serum. The irradiation process was conducted using a Xenon lamp at a wavelength of 700 ± 6 nm for 5 minutes. Then, the cell viability was quantified by measuring the change of the WST-1 absorbance at 450 nm with the reference at 630 nm.

3.1.4 Establishment of Tumor-Bearing Mouse Model

Balb/c Scl-nu/nu male mice (4-6 weeks old) were obtained from Japan SLC Inc. (Shizuoka, Japan). All animal experiments were carried out following the protocols reviewed and approved by the Institutional Animal Care and Research Advisory Committee at the Faculty of Pharmaceutical Sciences, Hokkaido University, Sapporo, Japan (Registration Number: 16-0015). To establish a tumor-bearing mouse model, SAS cells with a density of 1 x 10^6 cells in 80 μL PBS were subcutaneously injected into the right flank of the mouse. The tumor growth was monitored and measured by calipers using the following formula:

$$\text{Tumor volume } (mm^3) = 0.52 \times \text{long axis (mm)} \times \text{short axis}^2 \text{ (mm)}$$

3.1.5 Evaluation of PDT Antitumor Activity

After the tumor volume reached 50 mm^3 or six days after tumor inoculation, the mice randomized into five groups and separately treated by intratumoral administration of HEPES buffer containing 290 mM glucose pH 7.4 (HBG) with light irradiation (+ L), empty MITO-Porter + L, free rTPA + L, rTPA-MITO-Porter, and rTPA-MITO-Porter + L. The rTPA dose was fixed at 8.2 μg/mouse for all treatments containing rTPA. The light irradiation process was performed using a Xenon lamp with the optical filter that produces 700 ± 6 nm light for 20 minutes, 6h or 12h after the administration of the solution. The tumor growth was monitored every two days until the endpoint of the experiment (20 days after tumor cells inoculation). The relative tumor volume was calculated by comparing the tumor volume with its corresponding initial tumor volume prior to treatment.

3.1.6 Evaluation of Mitochondrial Membrane Potential

The mice received the rTPA-MITO-Porter (rTPA dose = 8.2 μg/mouse) and HBG (as negative control) *via* intratumoral administration followed by 700-nm light irradiation for 20 minutes, 12h after drug administration. The mice were sacrificed 3h after the light irradiation process, and tumor tissues were collected. The tumor tissues were incubated with 0.5 μM MitoProbe™ TMRM solution in PBS (-) for 30 minutes, followed by the observation using CLSM. The Olympus FV10i-LIV (Olympus Corporation, Tokyo, Japan) equipped with a water-immersion objective lens (UPlanSApo 60x/NA. 1.2) and a dichroic mirror (DM405/473/559/635) was used to detect the TMRM signal. The tissues were illuminated with 559 nm light to excite the TMRM, and the fluorescence detection channel was set using a filter at a bandpass 570-670 nm to detect TMRM fluorescence signal. The quantification of the mean fluorescence intensity of the TMRM was then performed from randomly-selected CLSM images using ImageJ software.

3.2 Results

3.2.1 Formulation Design for *In Vivo* Experiment

The rTPA-MITO-Porter system was further developed by replacing the SM with the Chol to obtain better particle integrity to be applied in the *in vivo* experiments. To achieve a suitable amount of the rTPA inside the MITO-Porter system, the total lipids' concentration was increased five times to 2.75 mM, without changing the molar ratio of each lipid component. The alteration on the total lipids' concentration effectively increased the amount of encapsulated-rTPA from 6.4 ± 2.2 μM to 37.6 ± 5.3 μM. The highly-positively charged nanoparticles with narrow size distribution were obtained, as shown in **Figure 3-1**. The particle size was slightly bigger compared to the low lipid content rTPA-MITO-Porter (**Table 2.1**), due to the use of high concentration of lipids. However, the particle size is on a suitable range for the *in vivo* application. Furthermore, the amount of rTPA inside the MITO-Porter system was also appropriate to be administered to the animal model.

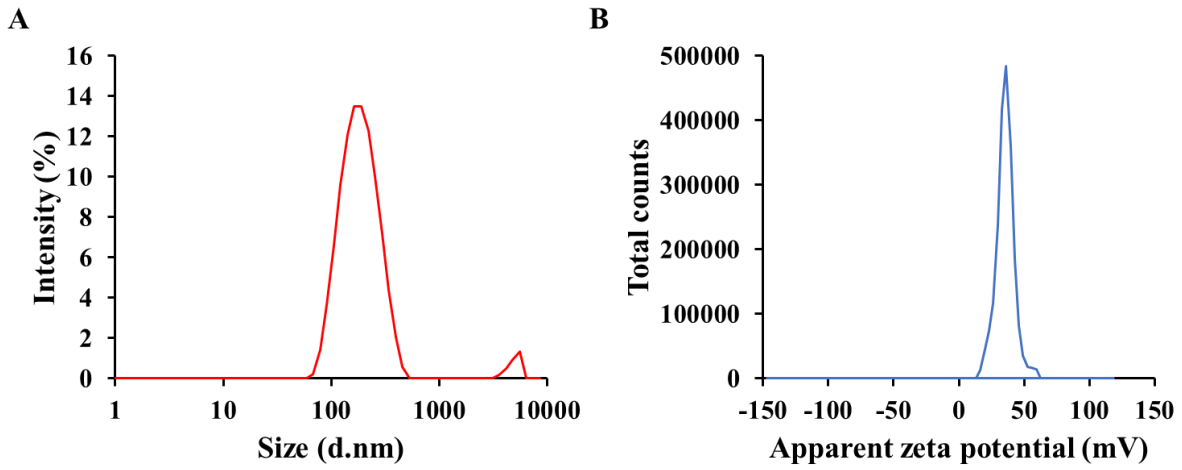

Figure 3-1 Particle characteristics of high lipid content rTPA-MITO-Porter*. A. particle size distribution (diameter = 169 ± 6 nm), with polydispersity index (PDI) of 0.22 ± 0.02; B. Zeta potential (36 ± 1 mV).*

3.2.2 Performance Verification of the rTPA-MITO-Porter

Due to the replacement of SM with Chol on the MITO-Porter formulation, the verification of the mitochondrial delivery ability is an important aspect to be pointed out. Therefore, to evaluate the mitochondrial accumulation level, the CLSM observation was conducted in SAS cell, as the potential target for PDT, and comparison was made between the rTPA-MITO-Porter containing SM with the rTPA-MITO-Porter containing Chol. All the particles were labeled with NBD dye, while the mitochondria were stained with MitoTracker™ Deep Red FM. As a result, the rTPA-MITO-Porter containing Chol exhibited similar mitochondrial accumulation profile corresponding to the rTPA-MITO-Porter containing SM, indicated by the appearance of several yellow signals, as the colocalization signal (**Figure 3-2**). It further validates that the replacement of the helper lipid is insignificantly affecting the mitochondrial delivery ability of the MITO-Porter system, as far as the DOPE and R8 are the main components of the MITO-Porter.

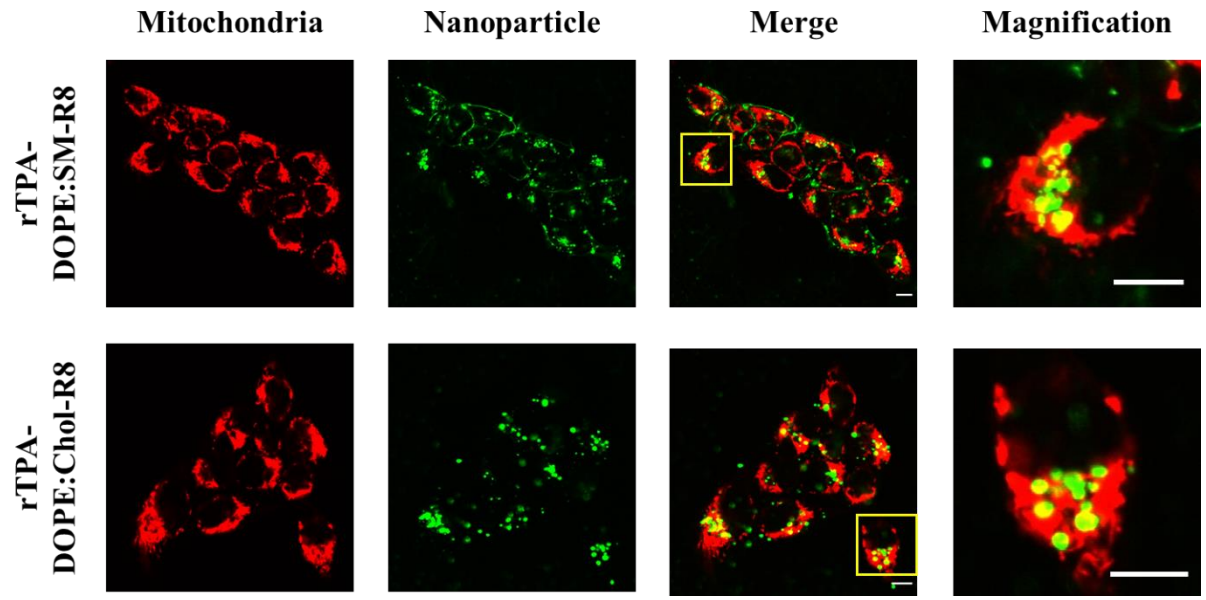

***Figure 3-2 The intracellular trafficking profile in SAS cells**. The alteration of helper lipid component from the SM to the Chol did not significantly affect the mitochondrial delivery ability of the rTPA-MITO-Porter. Scale bars: 10 μm.*

Another critical issue regarding the adjustment on the rTPA-MITO-Porter formulation is the effectivity of the system in inducing cytotoxicity during the photochemical reaction. The WST-1 assay was performed to evaluate the cytotoxicity of the high lipid content rTPA-MITO-Porter containing Chol against SAS cell, either in the absence or presence of light irradiation process. As shown in **Figure 3-3**, the combination of the rTPA-MITO-Porter with a 5 minutes irradiation process of the 700-nm light resulted in remarkable cytotoxicity against SAS cells, while negligible toxicity was obtained in the absence of light irradiation process. Furthermore, a dose-dependent toxicity profile was observed with the EC_{50} value of 0.27 ± 0.04 μM.

Based on the results mentioned above, the formulation adjustment on the rTPA-MITO-Porter system resulted in an insignificant alteration on the mitochondrial delivery ability. Moreover, the high lipid content rTPA-MITO-Porter with Chol produced a comparable phototoxicity profile to the low lipid content rTPA-MITO-Porter consisting of the SM, indicated by the EC_{50} value. Therefore, the high lipid content rTPA-MITO-Porter containing Chol is the best candidate to be applied for further translation process into the *in vivo* application.

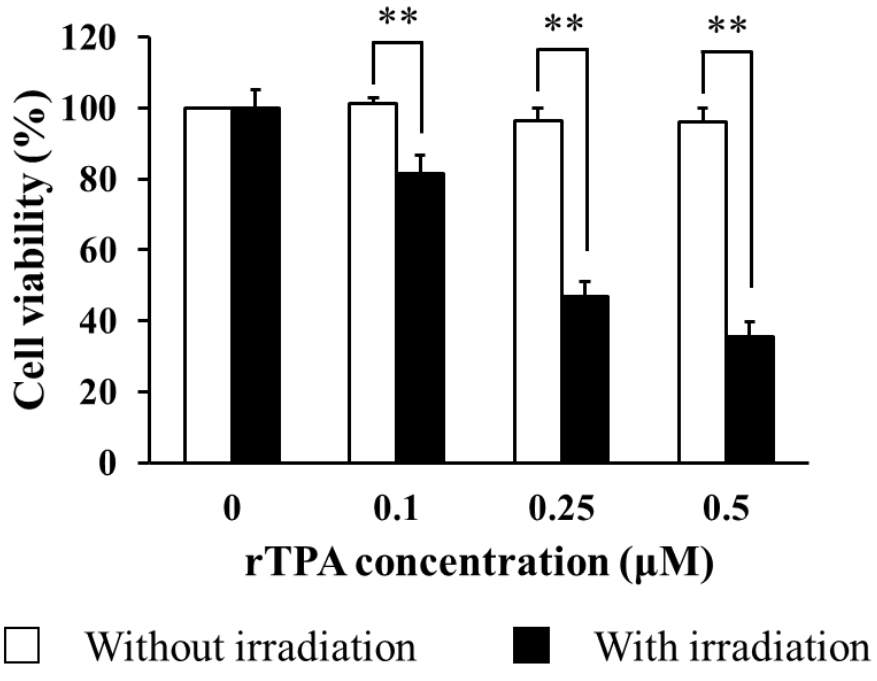

Figure 3-3 PDT toxicity of high lipid content rTPA-MITO-Porter against SAS cell*. The irradiation process was performed using 700 ± 6 nm light for 5 minutes with the density of 68.5 mW/cm^2. Data represent the average value of cell viability with S.D. (n =3; **p<0.01 by unpaired T-test).*

3.2.3 Evaluation of Antitumor Activity Against SAS Cells-bearing Mouse Model

After validating the mitochondrial delivery ability and *in vitro* PDT toxicity of the high lipid content rTPA-MITO-Porter with Chol, the investigation was continued by establishing human cancer engrafted on a mouse model. SAS cell was selected as the target in this evaluation for several reasons, as described in Chapter 2. The cells were inoculated subcutaneously into an immunodeficient mouse on the right flank. After the tumor volume reached 50 mm^3 or six days after tumor inoculation, the mice randomized into several treatment groups. Each group received specific treatment (rTPA dose = 8.2 μg/mouse) *via* intratumoral administration followed by 20 minutes light irradiation process using a Xenon lamp with the optical filter to produce 700 ± 6 nm light. The interval between drug administration and the light irradiation process or DLI (drug-light interval) was set to be 6 h. As shown in **Figure 3-4**, the rTPA-MITO-Porter exhibited notable inhibition on tumor growth in comparison to the negative control group that received HEPES buffer containing glucose with irradiation (HBG + L). However, three times the treatment of the rTPA-MITO-Porter with two days interval failed to produce better antitumor activity as opposed to a single treatment of the rTPA-MITO-Porter. It may be due to the interval between each treatment is too short, so that the harmful effects from multiple treatments are not clearly seen.

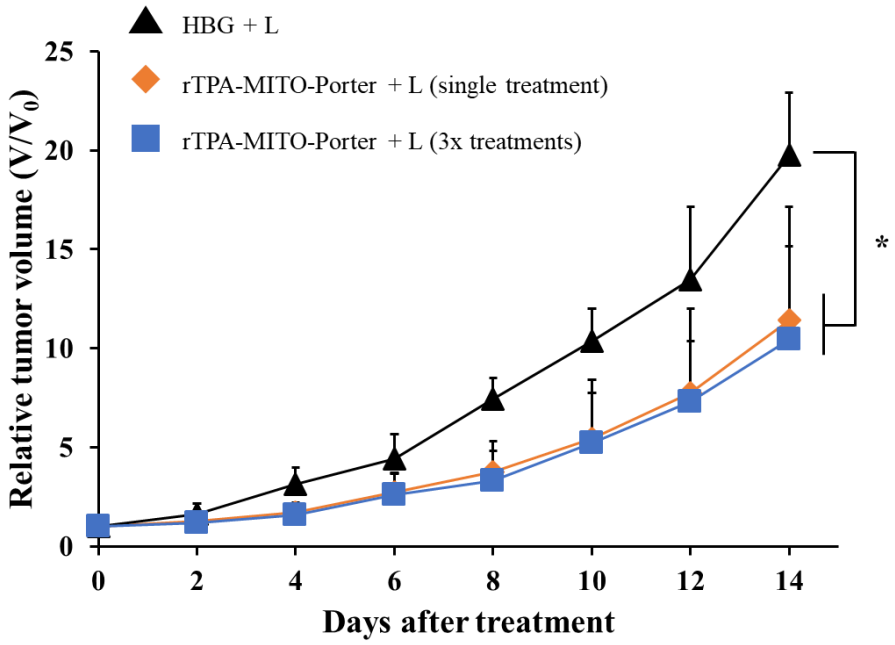

***Figure 3-4 Growth curves of SAS-bearing mouse on each group**. The graph indicates relative tumor volume compared to its corresponding initial tumor size before treatment. Data represent the average value with S.D. (n =3-5; *p<0.05 by ANOVA followed by Bonferroni).*

To further optimize the inhibition effect on the tumor growth, the DLI was prolonged into 12 h. The extension of this DLI is expected to facilitate the distribution of the particles in the tumor region. Furthermore, several control groups were added, including the rTPA-MITO-Porter without irradiation, empty MITO-Porter with irradiation, and free rTPA with irradiation. The evaluation was conducted using a single treatment process, with the same experimental design with the previous evaluation except in the DLI. As expected, treatment with the rTPA-MITO-Porter without irradiation and empty MITO-Porter with irradiation resulted in negligible antitumor activity (**Figure 3-5 A & C**). In contrast, efficient and significant inhibition of the tumor growth was observed in the group that received treatment of the rTPA-MITO-Porter with the irradiation process. Moreover, the antitumor activity of rTPA-MITO-Porter with 12 h DLI was relatively more potent than 6 h DLI, indicating the correlation between DLI and particle distribution.

Interestingly, the treatment of free rTPA with irradiation also produced an inhibition effect on tumor growth, as indicated by a slight decrease in the tumor volume at the end of the observation day. It could be associated with the ability of the rTPA in inducing the production of singlet oxygen during the photoirradiation process. However, the effectivity of the free rTPA in inhibiting tumor growth was significantly lower contrasted to the rTPA-MITO-Porter, indicating the importance of the MITO-Porter as a carrier system for optimizing the performance of the rTPA. Furthermore, there were no significant changes in the body weight of the animals during the treatment process (**Figure 3-5 B**), indicating the safety aspect of the treatment.

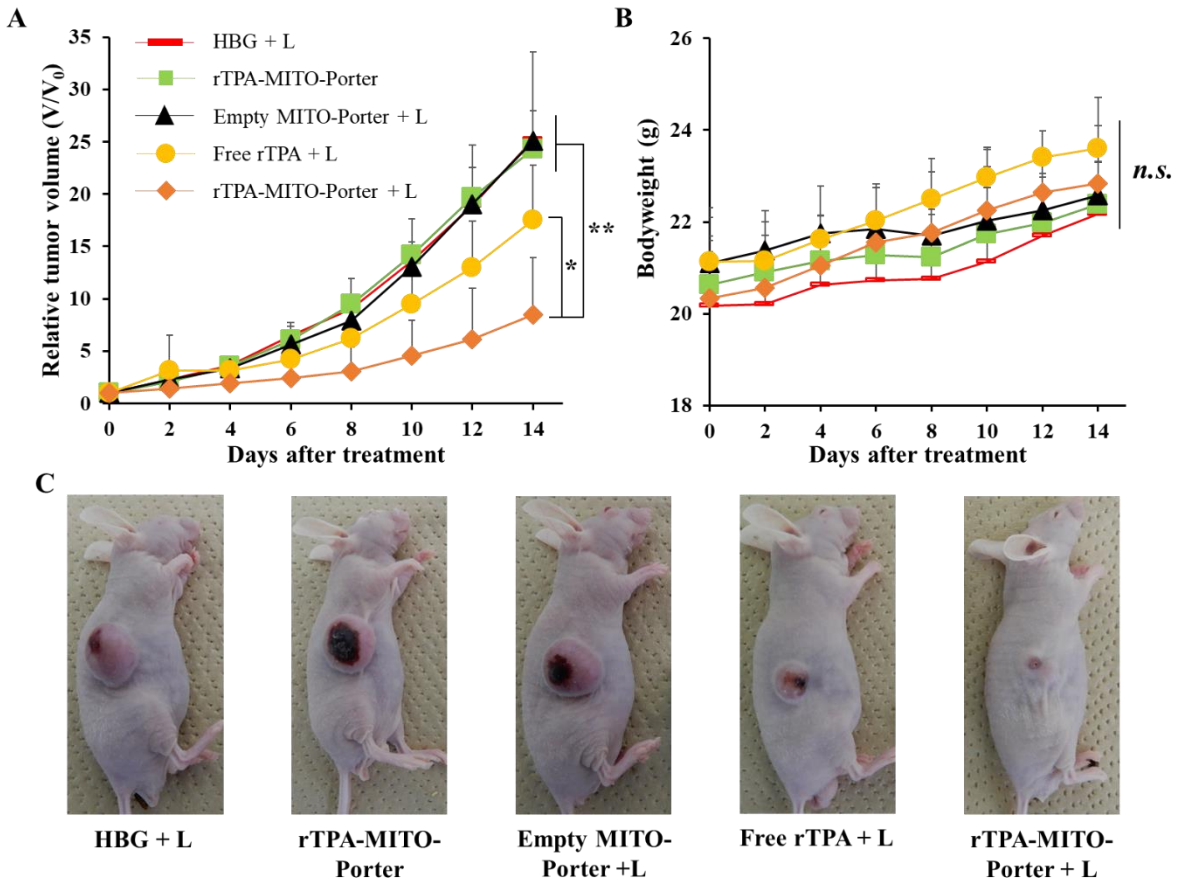

Figure 3-5 The antitumor evaluation using 12h DLI*. A. Tumor growth profiles of different treatment groups; B. The change in bodyweight during treatment; C. The representative photographs of SAS cell-bearing mice after receiving different treatments. The error bars indicate S.D. (n = 4-6, n.s. = not significant, *p<0.05, **p<0.01 by ANOVA followed by SNK-test).*

3.2.4 Evaluation of PDT-induced Mitochondrial Damage

After obtaining a remarkable antitumor activity through a single PDT treatment, the investigation was continued by evaluating the effect of the PDT process on the mitochondrial membrane potential of tumors. This evaluation was performed using tetramethylrhodamine methyl ester (TMRM), a specific fluorescence probe for the detection of mitochondrial membrane potential status. This probe can effectively accumulate in the negatively charge polarized mitochondria and produce a strong red-orange fluorescent signal upon excitation. When the mitochondrial membrane becomes depolarized, the probe is dispersed in the cytosol, and the fluorescent signal significantly diminishes.

In this evaluation, tumor tissues from the rTPA-MITO-Porter and HBG treated mice were collected and stained with TMRM solution, followed by CLSM observation to detect the

TMRM fluorescence signal. As shown in **Figure 3-6**, the intense red fluorescence signal of TMRM was observed in the HBG treated group, indicating the healthy mitochondrial condition. In contrast, the fluorescence signal was remarkably diminished after the PDT treatment of the rTPA-MITO-Porter, suggesting the decrease in mitochondrial membrane potential. The fluorescence intensity was further quantified using ImageJ software. As a result, the mean fluorescence intensity of TMRM was 1.9 times lower for the rTPA-MITO-Porter group in comparison to the HBG group. This result suggests that the PDT process of the rTPA-MITO-Porter effectively induced depolarization on the mitochondrial membrane. This result also further confirms that the photochemical reaction was localized inside the mitochondrial compartment of tumors.

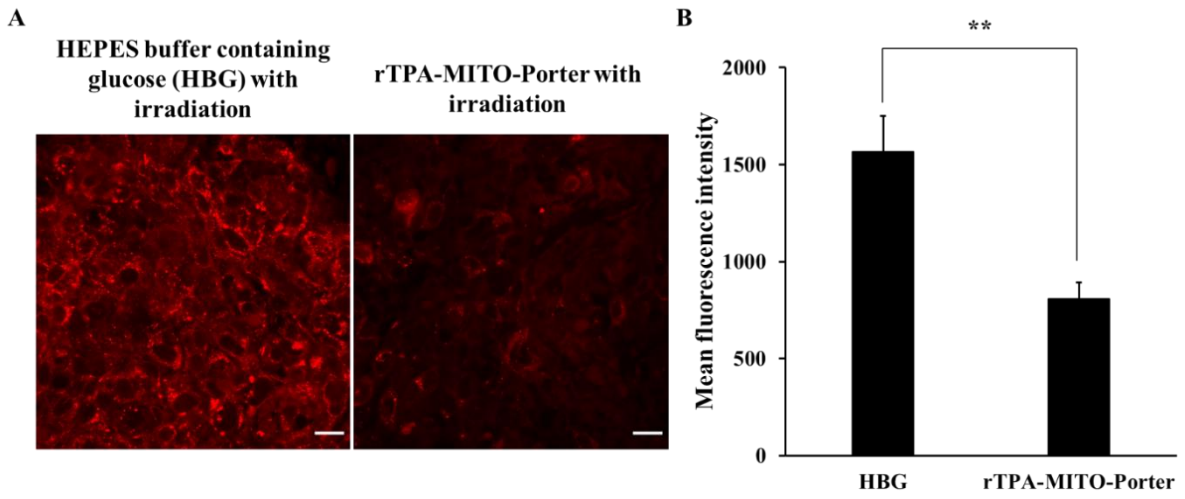

Figure 3-6 The mitochondrial membrane potential after PDT treatment*. A. The representative CLSM images of tumor tissues from mice treated by HBG and rTPA-MITO-Porter with 20 minutes light irradiation process; B. The mean fluorescence intensity of TMRM, calculated by ImageJ software from randomly selected CLSM images. Error bars indicate S.D. (n = 20, **p<0.01 by unpaired T-test).*

3.3 Discussion

In the previous chapter, the novel mitochondrial targeting PDT system has been successfully constructed with robust cell-killing capacity through the activation of the apoptosis cell death. Encouraged by that promising results, the translation process for the *in vivo* application further proceeded to evaluate the effectivity of this system in treating human tumor xenografted on the mouse model. In this study, the superficial type of human malignant cell, namely SAS cell, was chosen and inoculated subcutaneously on the immunodeficient mouse. The selection of an immunodeficient mouse was to minimize the rejection reaction by the mouse immune system toward the human cancer cell line. From the formulation design process, the alteration on the helper lipid composition and the total lipids' concentration produced in insignificant changes on the particle size and surface characteristics. Furthermore, the amount of encapsulated rTPA inside the MITO-Porter system was significantly increased by more than 5-folds to 37.6 ± 5.3 μM, which is suitable for the *in vivo* application.

Before evaluating the antitumor activity of this high lipid content rTPA-MITO-Porter containing Chol, several *in vitro* evaluation processes were conducted to verify the mitochondrial targeting ability and the phototoxicity profile of the particle. Based on the *in vitro* intracellular trafficking study and cytotoxicity evaluation on SAS cells, it was found that the alteration on the rTPA-MITO-Porter formulation did not affect the mitochondrial targeting ability and its phototoxicity profile. Therefore, the high lipid content rTPA-MITO-Porter containing Chol was further adopted for the further *in vivo* antitumor evaluation.

The antitumor activity evaluation was conducted by administering the rTPA-MITO-Porter *via* intratumoral administration. This administration route was chosen due to the location of the target tumor on the surface of the body. Moreover, the local administration provides lower systemic effects caused by off-target accumulation. By using a 6 h interval between drug administration and light irradiation process or DLI, a significant inhibition on the tumor growth was observed in the mice group that received the rTPA-MITO-Porter treatment.

In the ideal condition, the antitumor effects of PDT derive from three inter-related mechanisms of the direct killing effect through tumor cell necrosis or apoptosis, the shutdown of microvessels, and the activation of the immune response (19). However, in this PDT evaluation model, the effects mainly rely on the direct killing capacity of the rTPA towards tumor cells with an insignificant impact on the microvessels and negligible activation of the immune system due to the local administration and the use of an immunodeficient mouse, respectively. Based on this analysis, the distribution of the particles should be considered as

the most critical aspect of optimizing the cytotoxic effect. The prolong DLI may be required to facilitate better particle distribution inside the tumor region. Therefore, 12 h DLI was adopted for further antitumor activity evaluation.

By applying 12 h DLI, the more prominent cell killing capacity of the rTPA-MITO-Porter was obtained, as indicated by stronger suppression on the tumor growth as opposed to 6 h DLI and the other control groups. The robust antitumor activity of the rTPA-MITO-Porter was achieved by the specific localization of the photochemical reaction in the mitochondrial compartment of tumors. It was further reinforced by the finding of the depolarization on the mitochondrial membrane during the PDT process of the rTPA-MITO-Porter, as indicated by the significantly diminish of the TMRM fluorescence signal.

3.4 Summary and Conclusion

The rTPA-MITO-Porter consisting of DOPE and Chol with the total lipids' concentration of 2.75 mM and 10 mol% R8 was observed to be the best candidate for the PDT *in vivo* application. This particle exhibited comparable particle characteristics, mitochondrial targeting ability, and phototoxicity profile in comparison to its counterpart, which contains SM as the helper lipid with the total lipids' concentration of 0.55 mM. Based on the antitumor activity evaluation, a single PDT of the rTPA-MITO-Porter with the rTPA dose equivalent to 8.2 μg/mouse produced a remarkable antitumor activity with negligible systemic toxicity. Furthermore, the depolarization of the mitochondrial membrane was observed after the PDT process, suggesting the realization of mitochondrial delivery of the rTPA-MITO-Porter.

CHAPTER 4

Conclusion and Future Perspective

CHAPTER 4
CONCLUSION AND FUTURE PERSPECTIVE

4.1 General Conclusion

A novel mitochondrial targeting PDT system, namely the rTPA-MITO-Porter, has been successfully constructed by the incorporation of a π-extended porphyrin-type photosensitizer, namely rTPA, into a MITO-Porter system. The synergistic combination between these two components leads to remarkable cell-killing capacity by inducing the activation of the apoptosis cell death. The relatively low EC_{50} value was obtained against two different types of human cancer cell lines, indicating the effectivity of this system. Furthermore, the notable antitumor activity was observed by utilizing a single PDT process of the rTPA-MITO-Porter with minimal systemic toxicity, as indicated by the negligible alteration of the bodyweight of the mice during the treatment. The inhibition of the tumor growth mainly derives from the direct killing effect of the rTPA-MITO-Porter towards the malignant tissues. Additionally, the depolarization of the mitochondrial membrane was detected after the PDT process of the rTPA-MITO-Porter, suggesting the specific localization of the photochemical reaction inside the mitochondrial compartment of tumor tissues as well as the recognition of the mitochondrial delivery of the rTPA compound. Finally, this novel mitochondrial targeting PDT system demonstrates a promising feature for treating the superficial-type cancer cells through the photochemical reaction process.

4.2 Future Perspective

As was mentioned in Chapter 3, the PDT effect could be derived from three interrelated mechanisms, i.e., the direct killing effect, the shutdown of microvessels, and the activation of the immune response. In this study, the PDT effect mainly relied on the direct killing effect of the rTPA-MITO-Porter during the photoirradiation process through the production of an excessive amount of singlet oxygen, specifically in the mitochondria of tumor tissues. The activation of the other two mechanisms could further improve the PDT effectivity. It could be accomplished by using systemic administration of the rTPA-MITO-Porter in the immunocompetent mouse model. Therefore, further formulation design is needed to improve the blood circulation and tumor accumulation profile of the rTPA-MITO-Porter system. For

example, the introduction of polyethylene glycol (PEG) or several tumor-specific ligands on the surface of the rTPA-MITO-Porter can be a promising strategy for improving tumor accumulation profile after systemic administration. Lastly, the activation of the immune response during the PDT process could be evaluated by using an immunocompetent mouse model.

[REFERENCES]

1. Finkel T. **Signal transduction by reactive oxygen species**. *J Cell Biol*. **194**. 7-15 (2011).
2. Wiseman H, Halliwell B. **Damage to DNA by reactive oxygen and nitrogen species: Role in inflammatory disease and progression to cancer**. *Biochem J*. **313**. 17-29 (1996).
3. Trachootham D, Alexandre J, Huang P. **Targeting cancer cells by ROS-mediated mechanisms: A radical therapeutic approach?**. *Nat Rev Drug Discov*. **8**. 579–591 (2009).
4. Weinberg F, Hamanaka R, Wheaton WW, Weinberg S, Joseph J, Lopez M, Kalyanaraman B, Mutlu GM, Budinger GR, Chandel NS. **Mitochondrial metabolism and ROS generation are essential for Kras-mediated tumorigenicity**. *Proc Natl Acad Sci U S A*. **107**. 8788-8793 (2010).
5. Gamcsik MP, Kasibhatla MS, Teeter SD, Colvin OM. **Glutathione levels in human tumors**. *Biomarkers*. **17**. 671-691 (2012).
6. Karlenius TC, Tonissen KF. **Thioredoxin and cancer: A role for thioredoxin in all states of tumor oxygenation**. *Cancers*. **2**. 209-232 (2010).
7. Yoo MH, Xu XM, Carlson BA, Gladyshev VN, Hatfield DL. **Thioredoxin reductase 1 deficiency reverses tumor phenotype and tumorigenicity of lung carcinoma cells**. *J Biol Chem*. **281**. 13005-13008 (2006).
8. Hawk MA, McCallister C, Schafer ZT. **Antioxidant activity during tumor progression: A necessity for the survival of cancer cells?**. *Cancers*. **8**. 92 (2016).
9. Harris IS, Treloar AE, Inoue S, Sasaki M, Gorrini C, Lee KC, et al. **Glutathione and Thioredoxin Antioxidant Pathways Synergize to Drive Cancer Initiation and Progression**. *Cancer Cell*. **27**. 211-222 (2015).
10. Piskounova E, Agathocleous M, Murphy MM, Hu Z, Huddlestun SE, Zhao Z, et al. **Oxidative stress inhibits distant metastasis by human melanoma cells**. *Nature*. **527**. 186-191 (2015).
11. Gal K Le, Ibrahim MX, Wiel C, Sayin VI, Akula MK, Karlsson C, et al. **Antioxidants can increase melanoma metastasis in mice**. *Sci Transl Med*. **7**. 308re8 (2015).

12. Sayin VI, Ibrahim MX, Larsson E, Nilsson JA, Lindahl P, Bergo MO. **Cancer: Antioxidants accelerate lung cancer progression in mice**. *Sci Transl Med*. **6**. 221ra15 (2014).
13. Trachootham D, Zhou Y, Zhang H, Demizu Y, Chen Z, Pelicano H, et al. **Selective killing of oncogenically transformed cells through a ROS-mediated mechanism by β-phenylethyl isothiocyanate**. *Cancer Cell*. **10**. 241-252 (2006).
14. Wang J, Luo B, Li X, Lu W, Yang J, Hu Y, Huang P, Wen S. **Inhibition of cancer growth in vitro and in vivo by a novel ROS-modulating agent with ability to eliminate stem-like cancer cells**. *Cell Death Dis*. **8**. e2887 (2017).
15. Pelicano H, Feng L, Zhou Y, Carew JS, Hileman EO, Plunkett W, Keating MJ, Huang P. **Inhibition of mitochondrial respiration: A novel strategy to enhance drug-induced apoptosis in human leukemia cells by a reactive oxygen species-mediated mechanism**. *J Biol Chem*. **278**. 37832-37839 (2003).
16. Dougherty TJ, E KJ, Goldfarb A, Weishaupt KR, Boyle D, Mittleman A. **Photodynamic therapy for the treatment of malignant tumors**. *Can Res*. **38**. 2628-2635 (1978).
17. Dolmans DEJGJ, Fukumura D, Jain RK. Photodynamic therapy for cancer. *Nat Rev Cancer*. **3**. 380-387 (2003).
18. Daniell MD, Hill JS. **A history of photodynamic therapy**. *Aust N Z J Surg*. **61**. 340-348 (1991).
19. Castano AP, Demidova TN, Hamblin M. **Mechanisms in photodynamic therapy: part one**. *Photodiagnosis Photodyn Ther*. **1**. 279–293 (2004).
20. van Straten D, Mashayekhi V, de Bruijn HS, Oliveira S, Robinson DJ. **Oncologic photodynamic therapy: Basic principles, current clinical status and future directions**. *Cancers*. **9**. 19 (2017).
21. Baskaran R, Lee J, Yang S-G. **Clinical development of photodynamic agents and therapeutic applications**. *Biomater Res*. **22**. 25 (2018).
22. Abrahamse H, Hamblin MR. **New photossensitizersfot photodynamic therapy**. *Biochem J*. **473**. 347-364 (2017).
23. Agostinis P, Berg K, Cengel KA, Foster TH, Girotti AW, Gollnick SO, et al. **Photodynamic Terapy of cancer: un update**. *CA Cancer J Clin*. **61**. 250-281 (2012).
24. Dysart JS, Patterson MS. **Characterization of Photofrin photobleaching for singlet oxygen dose estimation during photodynamic therapy of MLL cells in vitro**. *Phys Med Biol*. **50**. 2597-2616 (2005).

25. Detty MR, Gibson SL, Wagner SJ. **Current Clinical and Preclinical Photosensitizers for Use in Photodynamic Therapy**. *J Med Chem*. **47**. 3897-3915 (2004).
26. O'Connor AE, Gallagher WM, Byrne AT. **Porphyrin and nonporphyrin photosensitizers in oncology: Preclinical and clinical advances in photodynamic therapy**. *Photochem Photobiol*. **85**. 1053-1074 (2009).
27. Brand MD, Affourtit C, Esteves TC, Green K, Lambert AJ, Miwa S, et al. **Mitochondrial superoxide: Production, biological effects, and activation of uncoupling proteins**. *Free Radic Biol Med*. **37**. 755-767 (2004).
28. Kurokawa H, Ito H, Inoue M, Tabata K, Sato Y, Yamagata K, et al. **High resolution imaging of intracellular oxygen concentration by phosphorescence lifetime**. *Sci Rep*. **5**. 10657 (2015).
29. Guo F, Yu M, Wang J, Tan F, Li N. **The mitochondria-targeted and IR780-regulated theranosomes for imaging and enhanced photodynamic/photothermal therapy**. *RSC Adv*. **6**. 11070-11076 (2016).
30. Mahalingam SM, Ordaz JD, Low PS. **Targeting of a Photosensitizer to the Mitochondrion Enhances the Potency of Photodynamic Therapy**. *ACS Omega*. **3**. 6066-6074 (2018).
31. Lv W, Zhang Z, Zhang KY, Yang H, Liu S, Xu A, et al. **A Mitochondria-Targeted Photosensitizer Showing Improved Photodynamic Therapy Effects Under Hypoxia**. *Angew Chemie - Int Ed*. **55**. 9947-9951 (2016).
32. Murphy MP. **Selective targeting of bioactive compounds to mitochondria**. *Trends Biotechnol*. **15**. 326-330 (1997).
33. Yamada Y, Akita H, Kamiya H, Kogure K, Yamamoto T, Shinohara Y, Yamashita K, Kobayashi H, Kikuchi H, Harashima H. **MITO-Porter: A liposome-based carrier system for delivery of macromolecules into mitochondria via membrane fusion**. *Biochim et Biophys Acta*. **1778**. 423-432 (2008).
34. Yamada Y, Harashima H. **Mitochondrial drug delivery systems for macromolecule and their therapeutic application to mitochondrial diseases**. *Adv Drug Deliv Rev*. **60**. 1439-1462 (2008).
35. Khalil IA, Kogure K, Futaki S, Harashima H. **High density of octaarginine stimulates macropinocytosis leading to efficient intracellular trafficking for gene expression**. *J Biol Chem*. **281**. 3544-3551 (2006).

36. Yamada Y, Fukuda Y, Harashima H. **An analysis of membrane fusion between mitochondrial double membranes and MITO-Porter, mitochondrial fusogenic vesicles**. *Mitochondrion*. **24**. 50-55 (2015).
37. Takano Y, Munechika R, Biju V, Harashima H, Imahori H, Yamada Y. **Optical control of mitochondrial reductive reactions in living cells using an electron donor-acceptor linked molecule**. *Nanoscale*. **9**. 18690-18698 (2017).
38. Sternberg ED, Dolphin D, Brückner C. **Porphyrin-based photosensitizers for use in photodynamic therapy**. *Tetrahedron*. **54**. 4151-4202 (1998).
39. Takano Y, Numata T, Fujishima K, Miyake K, Nakao K, Grove WD, et al. **Optical control of neuronal firing: Via photoinduced electron transfer in donor-acceptor conjugates**. *Chem Sci*. **7**. 3331-3337 (2016).
40. Andreoni A, Cubeddu R, De Silvestri S, Laporta P, Jori G, Reddi E. **Hematoporphyrin derivative: experimental evidence for aggregated species**. *Chem Phys Lett*. **88**. 33-36 (1982).
41. Moreira LM, Dos Santos FV, Lyon JP, Maftoum-Costa M, Pacheco-Soares C, Soares Da Silva N. **Photodynamic therapy: Porphyrins and phthalocyanines as photosensitizers**. *Aust J Chem*. **61**. 741-754 (2008).
42. TAnielian C, HEINRICH G. **Effect of aggregation on the hematoporphyrin-sensitized production of singlet molecular oxygen**. *Photochem Photobiol*. **61**. 131-135 (1995).
43. Bangham AD, Horne RW. **Negative staining of phospholipids and their structural modification by surface-active agents as observed in the electron microscope**. *J Mol Biol*. **8**. 660-668 (1964).
44. Papahadjopoulos D. **Liposomes as Drug Carriers**. *Annu Rep Med Chem*. **14**. 250-260 (1979).
45. Akbarzadeh A, Rezaei-Sadabady R, Davaran S, Joo SW, Zarghami N, Hanifehpour Y, et al. **Liposome: Classification, preparation, and applications**. *Nanoscale Res Lett*. **8**. 102 (2013).
46. Bozzuto G, Molinari A. **Liposomes as nanomedical devices**. *Int J Nanomedicine*. **10**. 975-999 (2015).
47. Kim S, Fujitsuka M, Majima T. **Photochemistry of singlet oxygen sensor green**. *J Phys Chem B*. **117**. 13985-13992 (2013).

48. Kim S, Tachikawa T, Fujitsuka M, Majima T. **Far-red fluorescence probe for monitoring singlet oxygen during photodynamic therapy**. *J Am Chem Soc*. **136**. 11707-11715 (2014).
49. Zorov DB, Filburn CR, Klotz LO, Zweier JL, Sollott SJ. **Reactive oxygen species (ROS)-induced ROS release: a new phenomenon accompanying induction of the mitochondrial permeability transition in cardiac myocytes**. *J Exp Med*. **192**. 1001-1014 (2000).
50. Yamada Y, Nakamura K, Furukawa R, Kawamura E, Moriwaki T, Matsumoto K, et al. **Mitochondrial delivery of bongkrekic acid using a MITO-porter prevents the induction of apoptosis in human hela cells**. *J Pharm Sci*. **102**. 1008-1015 (2013).
51. Yamada Y, Hashida M, Harashima H. **Hyaluronic acid controls the uptake pathway and intracellular trafficking of an octaarginine-modified gene vector in CD44 positive- and CD44 negative-cells**. *Biomaterials*. **52**. 189-198 (2015).
52. Schindelin J, Arganda-carreras I, Frise E, Kaynig V, Pietzsch T, Preibisch S, et al. **Fiji: an open-source platform for biological-image analysis**. *Nat Methods*. **9**. 676-682 (2012).
53. Adler J, Parmryd I. **Quantifying colocalization by correlation: The pearson correlation coefficient is superior to the Mander's overlap coefficient**. *Cytom Part A*. **77**. 733-742 (2010).
54. Chennoufi R, Bougherara H, Gagey-Eilstein N, Dumat B, Henry E, Subra F, et al. **Mitochondria-targeted Triphenylamine Derivatives Activatable by Two-Photon Excitation for Triggering and Imaging Cell Apoptosis**. *Sci Rep*. **6**. 21458 (2016).
55. Soriano J, Mora-Espí I, Alea-Reyes ME, Pérez-García L, Barrios L, Ibáñez E, et al. **Cell death mechanisms in Tumoral and Non-Tumoral human cell lines triggered by photodynamic treatments: Apoptosis, necrosis and parthanatos**. *Sci Rep*. **7**. 41340 (2017).
56. Kessel D, Oleinick NL. **Chapter 1 Initiation of Autophagy by Photodynamic Therapy**. *Methods Enzymol*. **453**. 1-16 (2009).
57. Mroz P, Yaroslavsky A, Kharkwal GB, Hamblin MR. **Cell death pathways in photodynamic therapy of cancer**. *Cancers*. **3**. 2516-2539 (2011).
58. Mahalingam SM, Ordaz JD, Low PS. **Targeting of a Photosensitizer to the Mitochondrion Enhances the Potency of Photodynamic Therapy**. *ACS Omega*. **3**. 6066-6074 (2018).

59. Mitsunaga M, Ogawa M, Kosaka N, Rosenblum LT, Choyke PL, Kobayashi H. **Cancer cell-selective in vivo near infrared photoimmunotherapy targeting specific membrane molecules**. *Nat Med*. **17**. 1685-1691 (2011).
60. JF Kerr, AH Wyllie, AR Currie. **Apoptosis: A basic biological phenomenon with wide-ranging implications in tissue kinetics**. *Br J Cancer*. **26**. 239-257 (1972).
61. Taylor RC, Cullen SP, Martin SJ. **Apoptosis: Controlled demolition at the cellular level**. *Nat Rev Mol Cell Biol*. **9**. 231-241 (2008).
62. Qi T, Chen B, Wang Z, Du H, Liu D, Yin Q, et al. **A pH-Activatable nanoparticle for dual-stage precisely mitochondria-targeted photodynamic anticancer therapy**. *Biomaterials*. **213**. 119219 (2019).
63. Yu Z, Sun Q, Pan W, Li N, Tang B. **A Near-Infrared Triggered Nanophotosensitizer Inducing Domino Effect on Mitochondrial Reactive Oxygen Species Burst for Cancer Therapy**. *ACS Nano*. **9**. 11064-11074 (2015).
64. Futaki S, Nakase I. **Cell-Surface Interactions on Arginine-Rich Cell-Penetrating Peptides Allow for Multiplex Modes of Internalization**. *Acc Chem Res*. **50**. 2449-2456 (2017).
65. El-Sayed A, Khalil IA, Kogure K, Futaki S, Harashima H. **Octaarginine- and octalysine-modified nanoparticles have different modes of endosomal escape**. *J Biol Chem*. **283**. 23450-23461 (2008).
66. Farhood H, Serbina N, Huang L. **The role of dioleoyl phosphatidylethanolamine in cationic liposome mediated gene transfer**. *Biochim Biophys Acta*. **1235**. 289-295 (1995).
67. Ricchelli F, Gobbo S, Moreno G, Salet C, Brancaleon L, Mazzini A. **Photophysical properties of porphyrin planar aggregates in liposomes**. *Eur J Biochem*. **253**. 760-765 (1998).
68. Kirakci K, Zelenka J, Rumlová M, Cvačka J, Ruml T, Lang K. **Cationic octahedral molybdenum cluster complexes functionalized with mitochondria-targeting ligands: Photodynamic anticancer and antibacterial activities**. *Biomater Sci*. **7**. 1386-1392 (2019).
69. Tang PM, Liu XZ, Zhang DM, Fong WP, Fung KP. **Pheophorbide a based photodynamic therapy induces apoptosis via mitochondrial-mediated pathway in human uterine carcinosarcoma**. *Cancer Biol Ther*. **8**. 533-539 (2009).

70. Zhou Z, Liu J, Rees TW, Wang H, Li X, Chao H, et al. **Heterometallic Ru–Pt metallacycle for two-photon photodynamic therapy**. *Proc Natl Acad Sci*. **115**. 5664-5669 (2018).
71. Pereira PMR, Silva S, Bispo M, Zuzarte M, Gomes C, Girão H, et al. **Mitochondria-Targeted Photodynamic Therapy with a Galactodendritic Chlorin to Enhance Cell Death in Resistant Bladder Cancer Cells**. *Bioconjug Chem*. **27**. 2762-2769 (2016).
72. Thomas AP, Palanikumar L, Jeena MT, Kim K, Ryu JH. **Cancer-mitochondria-targeted photodynamic therapy with supramolecular assembly of HA and a water soluble NIR cyanine dye**. *Chem Sci*. **8**. 8351-8356 (2017).
73. Zhang D, Wen L, Huang R, Wang H, Hu X, Xing D. **Mitochondrial specific photodynamic therapy by rare-earth nanoparticles mediated near-infrared graphene quantum dots**. *Biomaterials*. **153**. 14-26 (2018).
74. Taratula O, Schumann C, Naleway MA, Pang AJ, Chon KJ, Taratula O. **A multifunctional theranostic platform based on phthalocyanine-loaded dendrimer for image-guided drug delivery and photodynamic therapy**. *Mol Pharm*. **10**. 3946-3958 (2013).
75. Machacek M, Demuth J, Cermak P, Vavreckova M, Hruba L, Jedlickova A, et al. **Tetra(3,4-pyrido)porphyrazines Caught in the Cationic Cage: Toward Nanomolar Active Photosensitizers**. *J Med Chem*. **59**. 9443-9456 (2016).
76. Vachova L, Machacek M, Kučera R, Demuth J, Cermak P, Kopecky K, et al. **Heteroatom-substituted tetra(3,4-pyrido)porphyrazines: A stride toward near-infrared-absorbing macrocycles**. *Org Biomol Chem*. **13**. 5608-5612 (2015).
77. Liu J, Chen Y, Li G, Zhang P, Jin C, Zeng L, et al. **Ruthenium(II) polypyridyl complexes as mitochondria-targeted two-photon photodynamic anticancer agents**. *Biomaterials*. **56**. 140-153 (2015).
78. Li X, Zheng BY, Ke MR, Zhang Y, Huang JD, Yoon J. **A tumor-pH-responsive supramolecular photosensitizer for activatable photodynamic therapy with minimal in vivo skin phototoxicity**. *Theranostics*. **7**. 2746-2756 (2017).
79. Pan D, Zhong X, Zhao W, Yu Z, Yang Z, Wang D, et al. **Meso-substituted porphyrin photosensitizers with enhanced near-infrared absorption: Synthesis, characterization and biological evaluation for photodynamic therapy**. *Tetrahedron*. **74**. 2677-2683 (2018).
80. Lei Z, Zhang X, Zheng X, Liu S, Xie Z. **Porphyrin-ferrocene conjugates for photodynamic and chemodynamic therapy**. *Org Biomol Chem*. **16**. 8613-8619 (2018).

81. Liu DZ, Chen WY, Tasi LM, Yang SP. **Microcalorimetric and shear studies on the effects of cholesterol on the physical stability of lipid vesicles**. *Colloids Surf A Physicochem Eng Asp*. **172**. 57-67 (2000).

82. Briuglia ML, Rotella C, McFarlane A, Lamprou DA. **Influence of cholesterol on liposome stability and on in vitro drug release**. *Drug Deliv Transl Res*. **5**. 231-242 (2015).